A Non-Isolated Multi Input Multi Output DC−DC Boost Converter For Electric Vehicle Applications

A Project Report

submitted by

N JAWAHARLAL

in partial fulfilment of the requirements
for the award of the degree of

MASTER OF TECHNOLOGY

DEPARTMENT OF ELECTRICAL ENGINEERING
INDIAN INSTITUTE OF TECHNOLOGY MADRAS.

JUNE 2018

THESIS CERTIFICATE

This is to certify that the thesis entitled **"A Nonisolated Multiinput Multioutput DC−DC Boost Converter For Electric Vehicle Applications"** submitted by **N Jawaharlal** to the Indian Institute of Technology, Madras for the award of the degree of Master of Technology is a bona fide record of the project work done by him under my supervision. The contents of this thesis, in full or in parts, have not been submitted to any other Institute or University for the award of any degree or diploma.

Place: Chennai
Date: 21.06.2018

Prof. Mahesh Kumar
Project Guide
Professor
Dept. of Electrical Engineering
IIT-Madras, 600 036

ACKNOWLEDGEMENTS

Foremost I thank God Almighty for giving me an opportunity, strength and endurance for completing my project.

I would like to express my sincere gratitude towards several people who enabled me to reach this far with their timely guidance, support and motivation.I wish to thank them whole heartedly.

I offer my earnest gratitude to my guide, Prof. Mahesh Kumar whose knowledge and dedication has inspired me to work efficiently on the project and I thank him for invaluable comments and suggestions throughout the course of this project.

I thank to Dr.Krishna S for his help in my course work and as my faculty advisor.

I would like to express my sincere respect and profound gratitude to Dr. Devendra Jalihal, Head of Electrical Engineering Department for supporting and providing the facilities for my project work.

I consider myself fortunate to work with a fun-loving yet sincere group of lab mates. I would like to thank Manik Pradhan, Leelakrishna, Pruthvi and Srikanth for making this journey enjoyable.

Finally, I would like to express my thanks to my parents and my uncle G.Sudhakar, without their support I would have never been able to aspire for this level of education.

ABSTRACT

KEYWORDS: DC−DC converters, Electric vehicle, Hybrid power system, multiple input,multiple output (MIMO), smallsignal modeling, State-Space averaging, Energy storage system (ESS).

A new nonisolated multi input, multi output dc-dc boost converter is proposed. This converter is applicable in hybridizing alternative energy sources in electric vehicles. In fact, by hybridization of energy sources, advantages of different sources are achievable. In this converter, the loads power can be flexibly distributed between input sources. Also, charging or discharging of energy storages by other input sources can be controlled properly. The proposed converter has several outputs with different voltage levels which makes it suitable for interfacing to multilevel inverters. Using of a multilevel inverter leads to reduction of voltage harmonics which, consequently, reduces torque ripple of electric motor in electric vehicles. Also, electric vehicles which using dc motor have at least two different dc voltage levels, one for ventilation system and cabin lightening and other for supplying electric motor. The proposed converter has just one inductor.

Depending on charging and discharging states of the energy storage system (ESS), two different power operation modes are defined for the converter. In order to design the converter control system, small-signal model for each operation mode is extracted. The validity of the proposed converter and its control performance are verified by simulation results for different operation conditions.

TABLE OF CONTENTS

LIST OF TABLES

LIST OF FIGURES

ABBREVIATIONS

MIMO	Multi Input Multi Output
EVs	Electrical Vehicles
FCs	Fuel cells
ESS	Electrical Storage Systems
PVSC	Pulsating Voltage Source Converter
PCSC	Pulsating Current Source Converter
CCM	Continuous Conduction Mode
DCM	Dis Continuous Conduction Mode
TF	Transfer Function

NOTATION

V_{02}	Voltage across the load one
V_{01}	Voltage across the load two
V_{in1}	Supply voltage source one
V_{in2}	Supply voltage source Two
C_1, C_2	Capacitors
R_1, R_2	Resistors
L	Inductor
D	Diode
D_1	Duty cycle
S_1	MOSFET as switch
I_L	Inductor current
I_{in1}	First source current
I_{in2}	Battery current
I_{c1}	Capacitor current one
I_{c2}	Second capcitor current
V_T	Total load voltage
T	Time period
f_s	Swiching frequency
$K_{lead}(S)$	Lead compensator
$K_{lag}(S)$	Lag compensator
I_b	Battery average current
$g_{11}(S)$	Transfer function
$g_{22}(S)$	Transfer function
$g_{33}(S)$	Transfer function
$\hat{i}_L(t)$	Small change in Inductor current
$\hat{v}_{01}(t)$	Small change in output V_{01}
$\hat{v}_{02}(t)$	Small change in output V_{02}
$\hat{d}_1(t)$	Small change in duty D_1
$\hat{d}_2(t)$	Small change in duty D_2
$\hat{d}_3(t)$	Small change in duty ratio D_3
$\hat{d}_4(t)$	Small change in duty ratio D_4

CHAPTER 1

INTRODUCTION

Incresing rapidly population and energy consumption in the world, increasing oil and natural gas prices, and the depletion of fossil fuels are justifiable reasons for using electrical vehicles (EVs) instead of fossil-fuel vehicles. The interest in developing the EVs with clean and renewable energy sources as a replacement for fossil-fuel vehicles has therefore steadily increased. The EVs are proposed as a potential and attractive solution for transportation applications to provide environmentally friendly operation with the usage of clean and renewable energy sources [1], [2]. In the EVs, the fuel cell (FC) stack usually used as clean energy source. The FCs are energy sources that directly convert the chemical energy reaction into the electrical energy.

Currently, FCs are acknowledged as one of the promising technologies to meet the future energy generation requirements. FCs generate electric energy, rather than storing it, and continue to deliver the energy, as long as the fuel supply is maintained. However, there are some well-known technical limitations to FCs: they have slow power transfer rate in transitory situations, and a high cost per watt. This case is the reason for which FCs are not used alone in the EVs to satisfy the load demands, particularly during startup and transient events. So, in order to solve these problems, usually FC is used with energy storage systems (ESSs) such as batteries or supercapacitor (SC). Furthermore, the association of FC and ESSs leads to a reduction of the hydrogen consumption of the FC [3]-[7]. FC and ESSs such as battery and SC have different voltage levels. So, to provide a specific voltage level for load and control power flow between input sources, using of a dc-dc converter for each of the input sources is need. Usage of a dc-dc converter for each of the input sources leads to increase of price, mass, and losses. Consequently, in hybrid power systems, multiinput dc-dc converters have been used. Multiinput converters have two main types, isolated multiinput dc-dc converters and nonisolated multiinput dc dc converters. In the following sections, two main types of multiinput converters are investigated.

In isolated multiinput dc-dc converters, high-frequency transformer is used in order to make electric isolation. Highfrequency transformer provides electric isolation and impedance matching between two sides of converter. In general, isolated dcdc converters use leakage inductance as energy storage for transferring power between two sides of converter. Usually isolated dcdc converters, in addition to high-frequency transformer, have high-frequency inverter and rectifier. The power flow between input and output sides is controlled by adjusting the phase shift angle between primary and secondary voltages of transformer [8]-[10]. Isolated dc-dc converters have several types such as half-bridge isolated converters, full-bridge isolated converters, boost half-bridge isolated converters, and combinational multiport isolated converters [11]-[13].

Due to using of transformer, isolated dc-dc converters are heavy and massive. These converters require inverters in input sides of transformer for conversion of input dc voltage to ac and also need rectifiers in outputs of transformer for conversion of ac voltage to dc. Therefore, in all input and output terminals of these converters, several switches are applied which leads to increase of cost and losses. Furthermore, transformer has losses in its core and windings. Because of the aforementioned drawbacks of isolated multiinput dcdc converters, usage of nonisolated multiinput dc-dc converters in electric vehicle applications seems more useful. In [14], a nonisolated multiinput dc dc converter which is derived from H-bridge structure has been proposed. In fact, by cascading two H-bridge with different dc link voltages, different voltages due to addition or subtraction of H-bridges outputs are accessible. Modes in which either output voltage of the H-bridges is negative are not considered here because they are related to bidirectional double-input converters, which were beyond the scope of paper. By eliminating the aforementioned nonuseful modes, a simplified double input dcdc converter is obtained. The advantage of this converter is its less number of passive elements, and its drawback is unsuitable control on the power which is drawn from input sources.

In [22], a new converter for power and energy management between battery, SC, and electric motor in an electric vehicle is proposed. In this converter, instead of two separate inductors as energy storage element, a coupled inductor is used. It is claimed that utilization of coupled inductors lead to 22%-26% volume reduction in comparison with two separated inductors. However, volume of coupled inductors is more than one inductor. Also, regeneration of brake energy to battery and SC in this converter is possible. In [23], a multiinput converter with just one inductor is proposed which is able to distribute load power between input sources. Also, in this converter, transferring power between sources is possible. In [25] and [26], a single inductor multioutput dc dc converter is proposed which can generate several different voltage levels in its outputs. The converter is controlled to regulate the output voltages at their desired values despite the load power variation or input voltage variation.

In [28] and [29], a nonisolated multiinput multioutput converter is introduced which has just one inductor. Using of large number of switches is drawback of this converter which caused low efficiency. Impossibility of energy transferring between input sources is other disadvantage of the proposed converter. A new multiinput multioutput nonisolated converter based on combination of a multiinput and a multioutput converter is proposed. The proposed converter compared to similar cases has less number of elements. This converter can control power flow between sources with each other and load. Also, proposed converter has several outputs that each one can have different voltage level.

1.1 Organization Of Thesis

Chapter 1 Provides introduction about multi input and multi output boost converter. A brief note on converter and its operation modes. A comparative study of the topologies in literature is given.

Chapter 2 In this Chapter we are going to discuss about converter structure and operation modes in battery charging and discharging condition and inductor and capacitor equations.

Chapter 3 In this Chapter Transfer functions of two operation modes of the converter will be discussed . As transfer functions in two operation modes of converter are different, consequently, for each mode, different controller is needed to be designed separately.

Chapter 4 In this Chapter discuss about builting transfer function of system and we analysed about system stability by using Bode plot. We have six transfer functions. For each transfer function, frequency-domain bode plot analysis is obtained by Matlab to design the system compensators. System compensators is provided desired steady-state error and sufficient phase margin,high stability.

Chapter 5 Presents the conclusion of the project work and the suggestions for the future scope of the work.

CHAPTER 2

CONVERTER STRUCTURE AND OPERATION MODES

2.1 Introduction

In this Chapter we are going to discuss about converter structure and operation modes in battery charging and discharging condition[9]-[11]. Switching operations of converter also we discuss, inductor and capacitor equations in each operation mode. The proposed conveter structure is as shown in the Fig. 2.1.

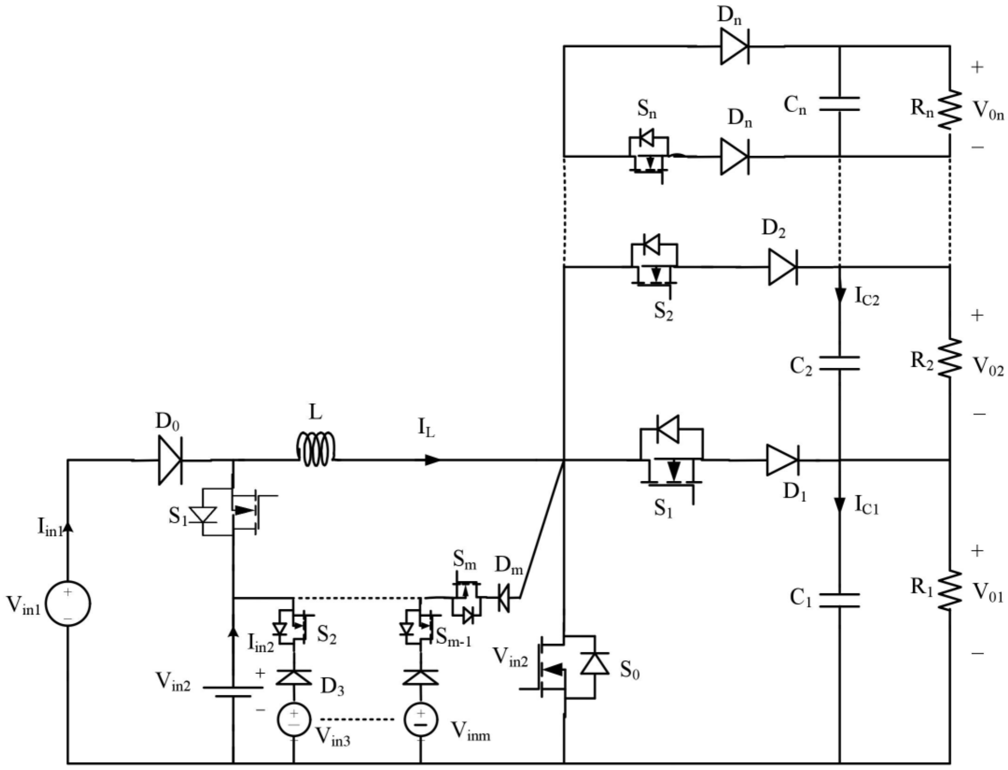

Figure 2.1: Proposed converter structure[11].

As mentioned in the Introduction, in [25], a multioutput converter is presented. The proposed converter is a single input converter. On the other hand, use of just one input energy source in electric vehicles cannot provide load requirements because the load is dynamic and its power has variation. Therfore, hybridization of different sources is essential.

As mentioned in the Introduction, in [23], a nonisolated multiinput dc-dc converter for hybridization of energy sources is proposed which has just one inductor. A nonisolated multiinput multioutput dc-dc converter based on the combination of these two converters is proposed. The structure of the proposed converter is presented in Fig. 1. As seen from the figure, the converter interfaces m input power sources V_{in1} ,V_{in2} ,V_{in3}, . . . , V_{inm} such that $V_{in1} < V_{in2} < V_{in3}... < V_{inm}$. The proposed converter has just one inductor, n capacitors in its outputs and m + n switches. The $R_1, R_2, R_3, ..., Rn$ are the load resistances, which can represent the equivalent power feeding a multilevel inverter.

By proper switching of switches, control of power flow between input sources in addition to boost up input sources voltages is possible. Outputs are capable to have different or equal voltage level which is appropriate for a connection to a multilevel inverter. The proposed converter is suitable alternative for hybridizing of FC, battery, or SC. For convenience, proposed converter with two-input two-output is analyzed.

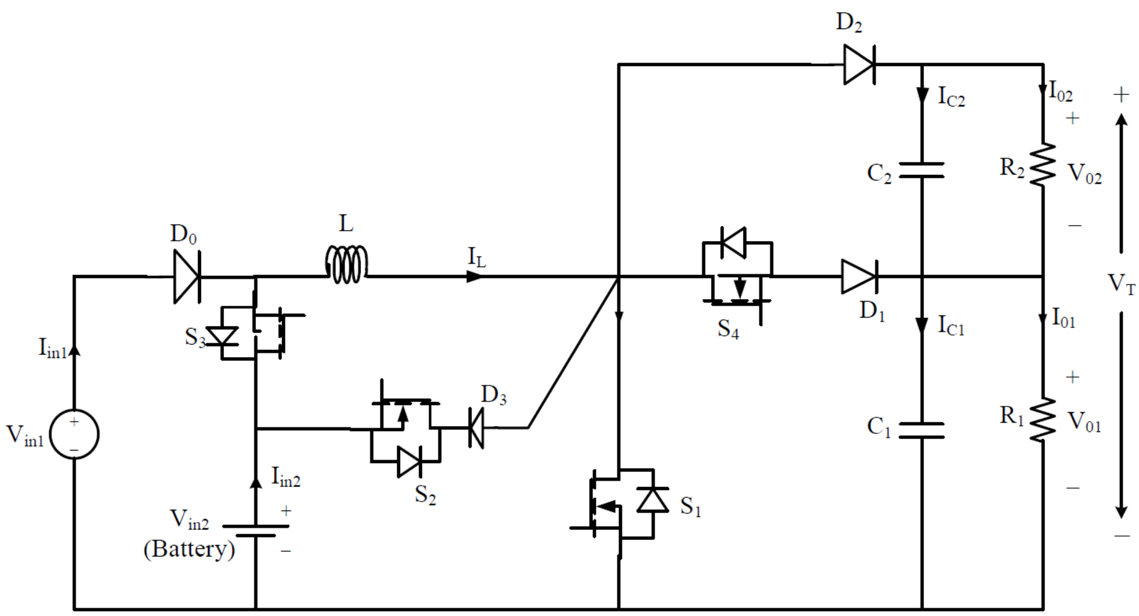

Figure 2.2: Proposed converter with two-input, two-output[11].

In Fig. 2.2, the proposed converter with two-input two-output is shown. In this figure, R_1 and R_2 are the model of load resistances that can represent the equivalent power feeding a multilevel inverter. Different types of multilevel inverters can be used in connection to this converter. Multilevel inverter which is used must be with nonfloating dc-links. Four power switches S_1,S_2,S_3,and S_4 in the converter structure are the main controllable elements that control the power flow and output voltages of the converter.

In the proposed converter, source V_{in1} can deliver power to source V_{in2} but not vice versa. So, in EV applications, FC which cannot be charged is located where V_{in1} is placed in circuit. Also, usually where V_{in2} is placed, ESSs such as battery or SC which are chargeable are located. FC is used as a generating power source and the battery is used as an ESS. Depending on the utilization state of the battery, two power operation modes are defined for proposed converter.

In each mode, just three of the four switches are active, while one switch is inactive. When load power is high,both input sources deliver power to load, in such a condition,S_2 is inactive and switches S_1,S_3,andS_4 are active. Also, when load power is low and V_{in2} is needed to be charged, V_{in1} not only supplies loads but also can charge V_{in2} . In this condition, switches S_1 ,S_2,and S_4 are active and S_3 is inactive. In FCs, because of output voltage dependence to drawn current and also to make an exact power balance among the input powers and the load, ripple of drawn current should be minimized.

Therefore, in this paper, steady state and dynamic behavior of the converter have been investigated in CCM. However, in battery charging mode when the loads power and battery charging current have low values, it is possible that the converter works in discontinuous conduction mode (DCM).

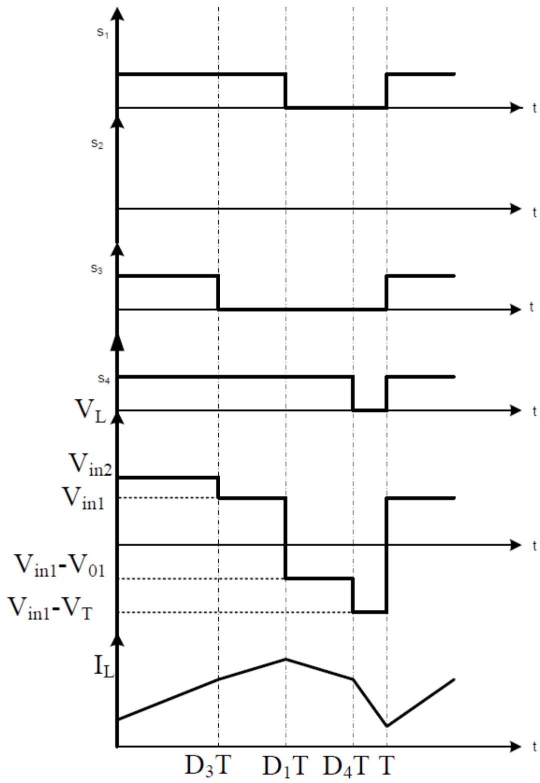

Figure 2.3: Steady-state waveforms of proposed converter in battery discharging mode[11].

So, the condition in which the converter goes to DCM is investigated in chapter 3. It should be noted that each of input sources can be used separately. In other words, the converter can work as a single input dcdc. Two main operation modes of the converter have been investigated as follows:

2.2 Battery Discharging mode

In this operation mode, two input power sources V_{in1} and V_{in2} (battery) are responsible for supplying the loads. In this mode, S_2 is OFF entirely and S_1, S_3, and S_4 are active. For each switch, a specific duty is considered[9]. Here, S_1 is active to regulate source 2 (battery) current to desired value. In fact, S_1 regulates battery current to desired value by controlling inductor current. Regulation of total output voltage $V_T = V_{O1} + V_{O2}$ to desired value is duty of the switch S_3 . Also, output voltage V_{O1} is controlled by S_4 . It is obvious that by regulation of V_T and V_{O1} , the output voltage V_{O2} is regulated too[11]. Gate signals of switches and also voltage and current waveforms of inductor are shown in Fig. 3. According to switches states, there are four different operation modes in one switching period as follows:

2.2.1 Switching State 1

$(0 < t < D_3T)$: In this state, switches S_1 and S_3 are turned ON. Because S_1 is ON, diodes D_1 and D_2 are reversely biased, so switch S_4 is turned OFF. Since S_3 is ON and $V_{in1} < V_{in2}$, diode D_0 is reversely biased. Equivalent circuit of proposed converter in this state is shown in Fig. 2.4 In this state, V_{in2} charges inductor L, so inductor current increases. Also, in this mode, capacitors C_1 and C_2 are discharged and deliver their stored energy to load resistances R_1 and R_2 , respectively.

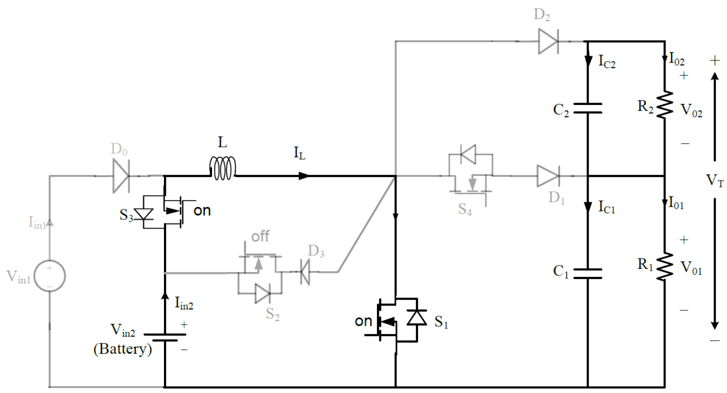

Figure 2.4: Switching state 1

The inductor and capacitors equations in this mode are as follows:

$$L\frac{di_L}{dt} = v_{in2} \tag{2.1}$$

$$C_1\frac{dv_{01}}{dt} = -\frac{v_{01}}{R_1} \tag{2.2}$$

$$C_2\frac{dv_{02}}{dt} = -\frac{v_{02}}{R_2} \tag{2.3}$$

2.2.2 Switching State 2

($D_3T < t < D_1T$): In this state, switch S_1 is still ON and S_3 is turned OFF. Because S_1 is ON, diodes D_1 and D_2 is reversely biased, so switch S_4 is still OFF. Equivalent circuit of proposed converter in this state is shown in Fig. 2.5 In this state, V_{in1} charges inductor L, so inductor current increases. In addition, capacitors C_1 and C_2 are discharged and deliver their stored energy to load resistances R_1 and R_2 , respectively.

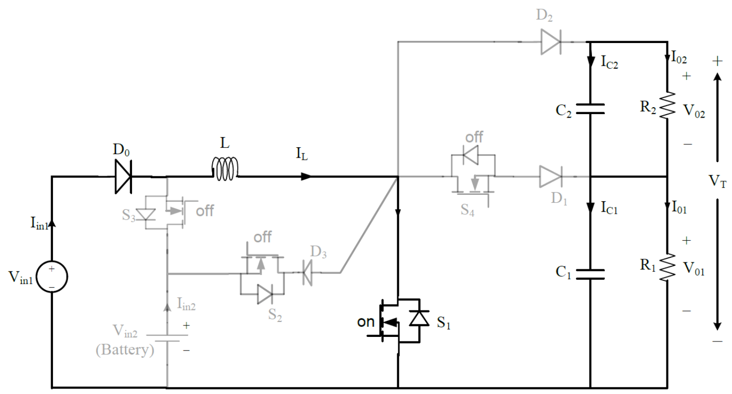

Figure 2.5: Switching state 2

The inductor and capacitors equations in this mode are as follows:

$$L\frac{di_L}{dt} = v_{in1} \tag{2.4}$$

$$C_1\frac{dv_{01}}{dt} = -\frac{v_{01}}{R_1} \tag{2.5}$$

$$C_2\frac{dv_{02}}{dt} = -\frac{v_{02}}{R_2} \tag{2.6}$$

2.2.3 Switching State 3

($D_1T < t < D_4T$): In this mode, switch S_1 is turned OFF and switch S_3 is still OFF. Also, switch S_4 is turned ON. Diode D_2 is reversely biased. Equivalent circuit of proposed converter in this state is shown in Fig. 2.6. In this state, inductor L is discharged and delivers its stored energy to C_1 and R_1 , so inductor current is decreased. In this state, C_1 is charged and C_2 is discharged and delivers its stored energy to load resistance R_2 . The energy storage elements L, C_1, and C_2 equations in this mode are as follows:

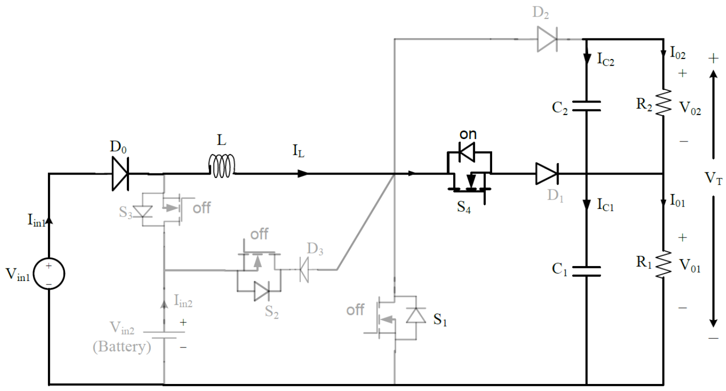

Figure 2.6: Switching state 3

The inductor and capacitors equations in this mode are as follows:

$$L\frac{di_L}{dt} = v_{in1} - v_{01} \tag{2.7}$$

$$C_1\frac{dv_{01}}{dt} = i_L - \frac{v_{01}}{R_1} \tag{2.8}$$

$$C_2\frac{dv_{02}}{dt} = -\frac{v_{02}}{R_2} \tag{2.9}$$

2.2.4 Switching State 4

($D_4T < t < T$): In this mode, all of three switches are OFF. So, diode D_2 is forward biased. In this state, inductor L is discharged and delivers its stored energy to capacitors C_1 , C_2 , and load resistances R_1 and R_2. Also, in this mode, capacitors C_1 and C_2 are charged. Equivalent circuit of proposed converter in this state is shown in Fig. 2.7

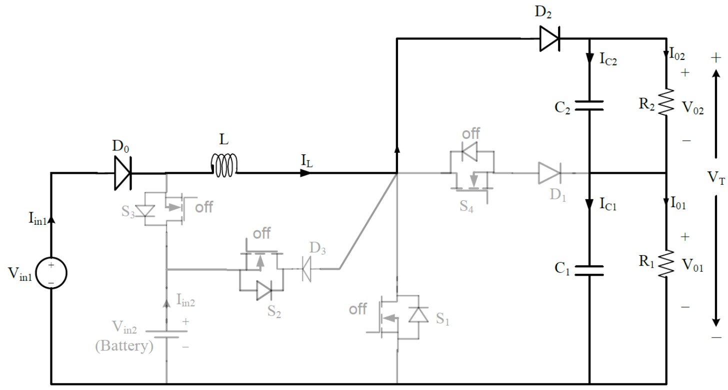

Figure 2.7: Switching state 4

The inductor and capacitors equations in this mode are as follows:

$$L\frac{di_L}{dt} = v_{in1} - (v_{01} + v_{02}) \tag{2.10}$$

$$C_1\frac{dv_{01}}{dt} = i_L - \frac{v_{01}}{R_1} \tag{2.11}$$

$$C_2\frac{dv_{02}}{dt} = i_L - \frac{v_{02}}{R_2} \tag{2.12}$$

2.3 Battery Charging mode

In this mode, V_{in1} not only supplies loads but also delivers power to V_{in2} (battery). This condition occurs when load power is low and battery requires to be charged. In this operation mode, switches S_1 , S_2 , and S_4 are active and switch S_3 is entirely OFF. Like previous operation mode of the converter in this mode, for each switch, a specific duty is considered. S_1 is switched to regulate total output voltage $V_T = V_O1 + V_O2$ to desired value.

Regulation of the battery charging current (Ib) to desired value is the duty of switch S_2 . Also, output voltage V_O1 is controlled by switch S_4 . It is clear that by regulation of V_T and V_{O1} , the output voltage V_{O2} is regulated too. In Fig. 2.8, gate signals of switches and voltage and current waveforms of inductor are shown. According to different switches states, there are four different operation modes in one switching period which is discussed as follows:

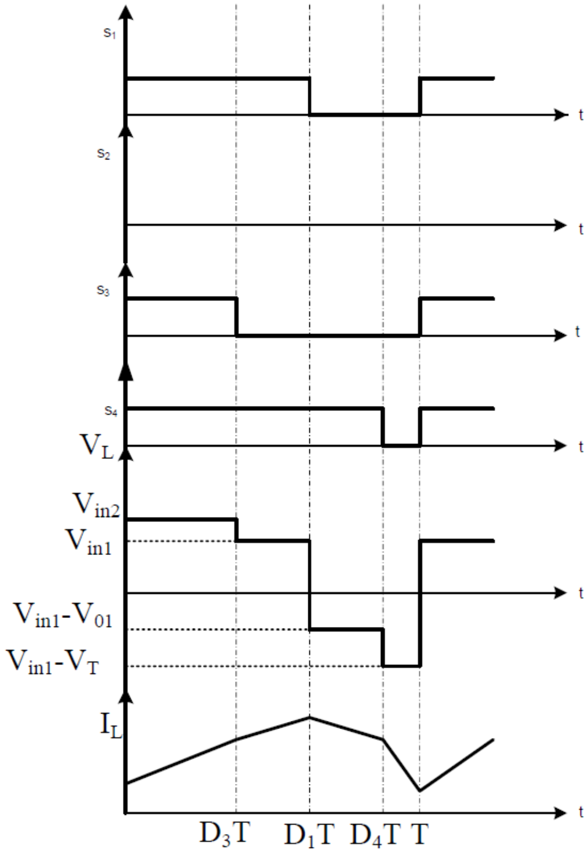

Figure 2.8: Steady-state waveforms of proposed converter in battery charging mode.[11]

2.3.1 Switching State 1

($0 < t < D_1T$): In this state, switch S_1 is turned ON, so S_2 and S_4 are reverse biased and cannot be turned ON. Also, diode D_2 is reversely biased and does not conduct. Equivalent circuit of proposed converter in this state is shown in Fig. 2.9 In this state, V_{in1} charges inductor L, so inductor current is increased. Also, in this mode, capacitors C_1 and C_2 are discharged and deliver their stored energy to load resistances R_1 and R_2 , respectively.

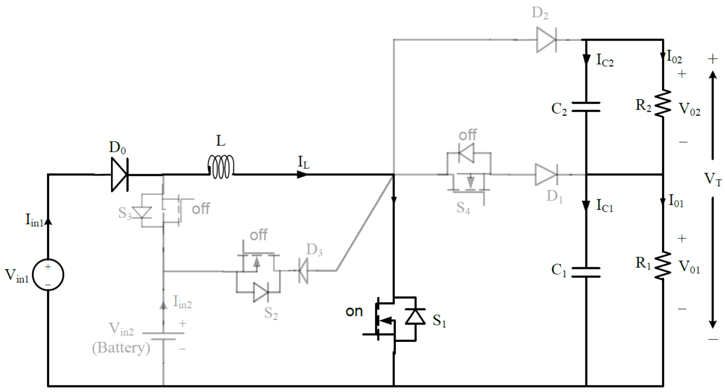

Figure 2.9: Switching state 1

The inductor and capacitors equations in this mode are as follows:

$$L\frac{di_L}{dt} = v_{in1}(2.13)$$

$$C_1\frac{dv_{01}}{dt} = -\frac{v_{01}}{R_1} \quad (2.14)$$

$$C_2\frac{dv_{02}}{dt} = -\frac{v_{02}}{R_2} \quad (2.15)$$

2.3.2 Switching State 2

$(D_1T < t < D_2T)$: In this mode, switch S_1 is turned OFF and switch S_2 is turned ON. Diode D_1 and D_2 are reversely biased, consequently, S_4 is still OFF. Equivalent circuit of proposed converter in this state is shown in Fig. 2.10. Since V_{in1} ¡ V_{in2} , therefore, in this period of time, inductor current decreases and inductor delivers its stored energy to battery (V_{in2}). Also, in this mode, capacitors C_1 and C_2 are discharged and deliver their stored energy to load resistancesR_1andR_2respectively.

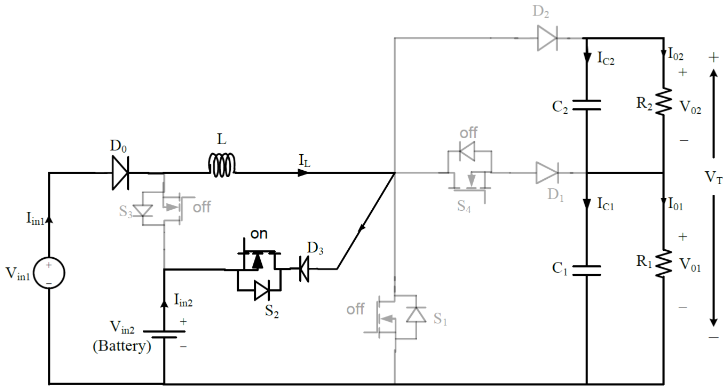

Figure 2.10: Switching state 2

The inductor and capacitors equations in this mode are as follows:

$$L\frac{di_L}{dt} = v_{in1} \tag{2.16}$$

$$C_1\frac{dv_{01}}{dt} = -\frac{v_{01}}{R_1} \tag{2.17}$$

$$C_2\frac{dv_{02}}{dt} = -\frac{v_{02}}{R_2} \tag{2.18}$$

2.3.3 Switching State 3

($D_2T < t < D_4T$): In this mode, switch $S_1$is still OFF and switch S_2 is turned OFF and switch $S_4$is turned ON. Also, diode$D_2$is reversely biased. In Fig. 2.11, equivalent circuit of proposed converter in this state is shown. In this state, inductor L is discharged and delivers its stored energy to C_1 and R_1, so inductor current is decreased. In this state, capacitors $C_1$is charged and capacitor C_2 is discharged and delivers its stored energy to load resistance R_2. The energy storage elements L, C_1,and C_2 respectively.

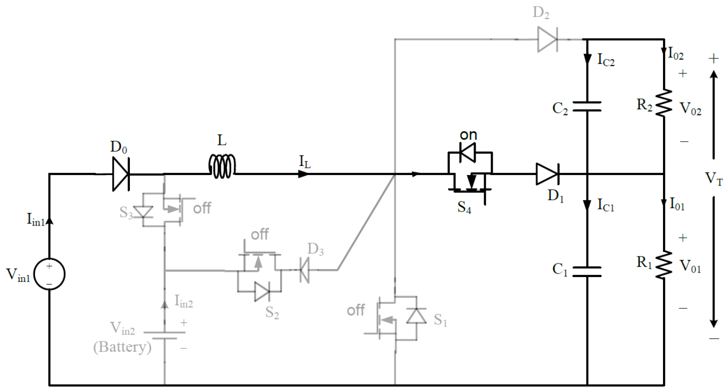

Figure 2.11: Switching state 3

The inductor and capacitors equations in this mode are as follows:

$$L\frac{di_L}{dt} = v_{in1} - v_{01} \tag{2.19}$$

$$C_1\frac{dv_{01}}{dt} = i_L - \frac{v_{01}}{R_1} \tag{2.20}$$

$$C_2\frac{dv_{02}}{dt} = -\frac{v_{02}}{R_2} \tag{2.21}$$

2.3.4 Switching State 4

($D_4T < t < T$): In this mode, all the three switches are OFF. Therefore, diode D_2 is forward biased. In Fig. 2.12, an equivalent circuit of the proposed converter in this state is shown. In this state, inductor L is discharged and delivers its stored energy to capacitors C_1, C_2, and loadresistances R_1 and R_2. Also, in this mode, capacitors C_1 and C_2 are charged.

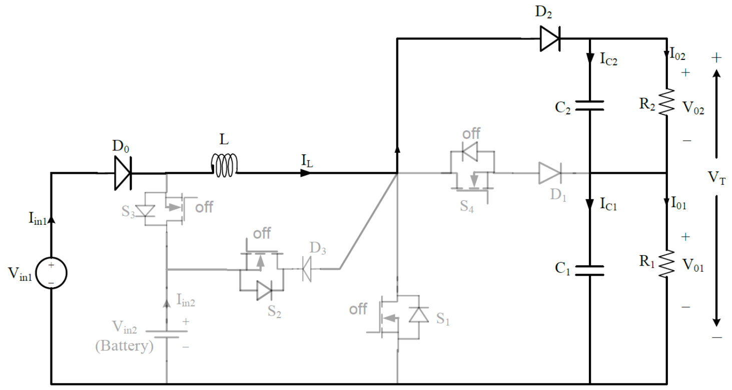

Figure 2.12: Switching state 4

The inductor and capacitors equations in this mode are as follows:

$$L\frac{di_L}{dt} = v_{in1} - (v_{01} + v_{02}) \tag{2.22}$$

$$C_1\frac{dv_{01}}{dt} = i_L - \frac{v_{01}}{R_1} \tag{2.23}$$

$$C_2\frac{dv_{02}}{dt} = i_L - \frac{v_{02}}{R_2} \tag{2.24}$$

2.4 Summery

In this Chapter we are going to discussed about converter structure and operation modes in battery charging and discharging condition. Switching operations of converter also we discussed, and also we came to know inductor and capacitor status in each operation mode.

CHAPTER 3

DYNAMIC MODELING OF THE PROPOSED CONVERTER

3.1 Introduction

As mentioned in pervious Chapter 2, the proposed converter is controlled by switches S_1 , S_2 , S_3 , and S_4 . Each switch has its own specific duty. By proper regulation of switches duty cycles, output voltages and battery charging or discharging current are adjustable[14]. To design the closed loop controller for the converter, first dynamic model must be obtained. As stated in previous Chapter, proposed converter has two main operation modes which in battery discharging mode two input sources deliver power to load and in battery charging mode, source V_{in1} not only supplies the load power but also charges V_{in2} (battery). There are different dynamic models for each operation modes of converter. Consequently, for both operation modes, different controller need to be designed separately.

3.2 Dynamic Model of Battery Discharging Mode

Small-signal model is the basis for optimized controller design. Especially, for such a multiinput multioutput converter, an effective model will be helpful to realize closed-loop control, and furthermore, to optimize the converter dynamics. Unlike conventional single input single output converter, the multiport converter is a high-order system, and the symbolic derivation of these plant transfer functions is fairly tedious; therefore, it is difficult to obtain values of poles and zeros for analysis. Alternatively, the dynamics of the plant can be described in a matrix form; therefore, computer software is used to plot the bode graph of different transfer functions. Based on small-signal modeling method [30], the state variables, duty ratios, and input voltages contain two components, dc values (X, D, V) and perturbations ($\hat{x}$,$\hat{d}$,$\hat{v}$). It is assumed that the perturbations are small and do not vary significantly during one switching period. So, there are following equation for proposed converter:

$$i_L(t) = I_L + \hat{i}_L(t) \tag{3.1}$$

$$v_{01}(t) = V_{01} + \hat{v}_{01}(t) \tag{3.2}$$

$$v_{02}(t) = V_{02} + \hat{v}_{02}(t) \tag{3.3}$$

$$d_1(t) = D_1 + \hat{d}_1(t) \tag{3.4}$$

$$d_2(t) = D_2 + \hat{d}_2(t) \tag{3.5}$$

$$d_3(t) = D_3 + \hat{d}_3(t) \tag{3.6}$$

$$d_4(t) = D_4 + \hat{d}_4(t) \tag{3.7}$$

Where inductor current $i_L(t)$ and capacitor voltages $v_{O1}(t)$ and $v_{O2}(t)$ are state variables. If we substitute (3.1) to (3.7)into (2.1) to (2.12), apply the averaging to four state equations multipliedwith corresponding duty cycle value, and then, neglect second-order terms, we obtain small-signal equations that are demonstrated as follows:

$$L\frac{d\hat{i}_L}{dt} = (V_{in2} - V_{in1})\hat{d}_3(t) + D_3\hat{v}_{in2}(t) + (1 - D_3)\hat{v}_{in1}(t) - (1 - D_1)\hat{v}_{01}(t)$$

$$+(\mathrm{D}_4 - 1)\hat{v}_{02}(t) + V_{01}\hat{d}_1(t) + V_{02}\hat{d}_4(t)(3.8)$$

$$C_1\frac{d\hat{v}_{01}(t)}{dt} = -I_L\hat{d}_1(t) + (1 - D_1)\hat{i}_L(t) - \frac{\hat{v}_{01}(t)}{R_1} \tag{3.9}$$

$$C_2\frac{d\hat{v}_{02}(t)}{dt} = -I_L\hat{d}_4(t) + (1 - D_4)\hat{i}_L(t) - \frac{\hat{v}_{02}(t)}{R_2} \tag{3.10}$$

Therefore, the system can be represented in a matrix form using a state-space model such that $i_L(t)$, $v_{O1}(t)$, and $v_{O2}(t)$ are state variables. The state-space model takes the following form:

$$\frac{dX}{dt} = AX + BU \tag{3.11}$$

$$Y = CX + DU \tag{3.12}$$

Where X is a matrix containing the state variables, U is a matrix containing the control inputs $d_1(t)$, $d_3(t)$ and $d_4(t)$, and Y is a matrix containing the system outputs $v_{O1}(t)$, $v_T(t)$, and $i_b(t)$. So, matrixes X, Y , U take following form:

$$\mathbf{X} = \begin{bmatrix} \hat{i}_L(t) \\ \hat{v}_{01}(t) \\ \hat{v}_{02}(t) \end{bmatrix} \tag{3.13}$$

,

$$\mathbf{Y} = \begin{bmatrix} \hat{v}_{01}(t) \\ \hat{v}_T(t) \\ \hat{i}_b(t) \end{bmatrix} \tag{3.14}$$

,

$$\mathbf{U} = \begin{bmatrix} \hat{d}_4(t) \\ \hat{d}_3(t) \\ \hat{d}_1(t) \end{bmatrix} \tag{3.15}$$

Filling in the A, B, C, and D matrices using (3.8) to (3.10) and state equations (3.11) and (3.12), gives the following result:

$$\mathbf{A} = \begin{bmatrix} 0 & \frac{(D_1-1)}{L} & \frac{(D_4-1)}{L} \\ \frac{(1-D_1)}{C_1} & -\frac{1}{R_1C_1} & 0 \\ \frac{(1-D_4)}{C_2} & 0 & -\frac{1}{R_2C_2} \end{bmatrix} \tag{3.16}$$

,

$$\mathbf{B} = \begin{bmatrix} \frac{(V_{02})}{L} & \frac{(V_{01})}{L} & \frac{V_{in2}-V_{in1}}{L} \\ 0 & -\frac{I_L}{C_1} & 0 \\ -\frac{I_L}{C_2} & 0 & 0 \end{bmatrix} \tag{3.17}$$

$$\mathbf{C} = \begin{bmatrix} 0 & 1 & 0 \\ 0 & 1 & 1 \\ D_3 & 0 & 0 \end{bmatrix} \tag{3.18}$$

,

$$\mathbf{D} = \begin{bmatrix} 0 & 0 & 0 \\ 0 & 0 & 0 \\ 0 & I_L & 0 \end{bmatrix} \tag{3.19}$$

Where V_{in1} and V_{in2} are input sources voltages. Also, V_{O1} and V_{O2} are output voltages. In the$A$, B, C, and D matrices, all parameters except duty cycle of switches D_1 , D_3 , D_4 , and dc value of inductor current I_L , are known. For the inductor current, there is the following equation:

$$I_L = \frac{I_b}{D_3} \tag{3.20}$$

Where I_b is the battery current. So, the only unknown parameters of expressed matrices are D_1 , D_3 , and D_4 . The values of switches duty cycles are obtained by steady-state equations which expressed in following equation:

$$\begin{bmatrix} V_{01} & V_{in2} - V_{in1} & V_{02} \\ R_1 I_b & V_{01} & 0 \\ 0 & V_{02} & R_2 I_b \end{bmatrix} \begin{bmatrix} D_1 \\ D_3 \\ D_4 \end{bmatrix} = \begin{bmatrix} V_{02} + V_{01} - V_{in1} \\ R_1 I_b \\ R_2 I_b \end{bmatrix} \tag{3.21}$$

So, from the aforementioned matrix equation, duty cycles of switches achieved and are placed inA,B, C, andDmatrices.As represented in the system small-signal models[14], state variables are controlled by three control variables $d_1(t)$, $d_3(t)$, and $d_4(t)$. The transfer function matrix of the converter is obtained from the small signal model as follows:

$$G = C(SI - A)^{-1}B + D \tag{3.22}$$

$$y = Gu \tag{3.23}$$

The rank of transfer function matrix denotes the number of control variables. In this paper, according to the number of control variables and based on X,Y,Z rank of transfer function matrix G

$$\begin{bmatrix} y_1 \\ y_2 \\ y_3 \end{bmatrix} = \begin{bmatrix} g_{11} & g_{12} & g_{13} \\ g_{21} & g_{22} & g_{23} \\ g_{31} & g_{32} & g_{33} \end{bmatrix} \begin{bmatrix} u_1 \\ u_2 \\ u_3 \end{bmatrix} \tag{3.24}$$

Where y and u are the system output and input vectors, and component $g_i j$ represents the transfer function between y_i and u_j . So, there are three transfer functions as follows:

$$\frac{\hat{v}_{01}(s)}{\hat{d}_4(s)} = g_{11} \tag{3.25}$$

$$\frac{\hat{v}_T(s)}{\hat{d}_3(s)} = g_{22} \tag{3.26}$$

$$\frac{\hat{i}_b(s)}{\hat{d}_1(s)} = g_{33} \tag{3.27}$$

3.3 Dynamic Model of Battery charging Mode

In this operation mode of proposed converter, which V_{in1} delivers energy to loads and V_{in2} (battery), switches S_1 , S_2 , and S_4 are active and switch S_3 is inactive. Like battery discharging mode, first small signal model should be obtained by substituting (3.1) to (3.7) into (2.13) to (2.24), apply the averaging to four state equations multiplied with corresponding duty cycle value, and then, neglect second-order terms, we obtain small-signal equations that are demonstrated as follows:

$$L\frac{d\hat{i}_L}{dt} = \hat{v}_{in1}(t) + V_{in2}\hat{d}_1(t) + (D_1 - D_2)\hat{v}_{in2}(t) + (V_{01} - V_{in2})\hat{d}_2(t) + V_{02}\hat{d}_4(t)$$

$$+(\mathrm{D}_2 - 1)\hat{v}_{01}(t) - (1 - D_4)\hat{v}_{02}(t) + (D_4 - 1)\hat{v}_{02}(t) + V_{01}\hat{d}_1(t) + V_{02}\hat{d}_4(t) \quad (3.28)$$

$$C_1\frac{d\hat{v}_{01}(t)}{dt} = -I_L\hat{d}_2(t) + (1 - D_2)\hat{i}_L(t) - \frac{\hat{v}_{01}(t)}{R_1} \quad (3.29)$$

$$C_2\frac{d\hat{v}_{02}(t)}{dt} = -I_L\hat{d}_4(t) + (1 - D_4)\hat{i}_L(t) - \frac{\hat{v}_{02}(t)}{R_2} \quad (3.30)$$

These equations can be expressed as state space equations. In this operation mode similar to battery discharging mode $i_L(t)$, $v_{O1}(t)$, and $v_{O2}(t)$ are the state variables. State variables, input, and output matrices are illustrated as follows:

$$\mathbf{y} = \begin{bmatrix} \hat{v}_{01}(t) \\ \hat{v}_T(t) \\ \hat{i}_b(t) \end{bmatrix}, \mathbf{X} = \begin{bmatrix} \hat{i}_L(t) \\ \hat{v}_{01}(t) \\ \hat{v}_{02}(t) \end{bmatrix}, \mathbf{u} = \begin{bmatrix} \hat{d}_4(t) \\ \hat{d}_1(t) \\ \hat{d}_2(t) \end{bmatrix} \quad (3.31)$$

Where $v_T(t) = v_{O1}(t) + v_{O2}(t)$. Finally for this operation mode of converter, similar to pervious mode, there are A, B, C, and D matrices as follows:

$$\mathbf{A} = \begin{bmatrix} 0 & \frac{(D_2-1)}{L} & \frac{(D_4-1)}{L} \\ \frac{(1-D_2)}{C_1} & -\frac{1}{R_1C_1} & 0 \\ \frac{(1-D_4)}{C_2} & 0 & -\frac{1}{R_2C_2} \end{bmatrix}, \mathbf{B} = \begin{bmatrix} \frac{(V_{in2})}{L} & \frac{(V_{01}-V_{in2})}{L} & \frac{V_{02}}{L} \\ 0 & -\frac{I_L}{C_1} & 0 \\ 0 & 0 & -\frac{I_L}{C_2} \end{bmatrix} \quad (3.32)$$

$$\mathbf{C} = \begin{bmatrix} 0 & 1 & 0 \\ 0 & 1 & 1 \\ D_2 - D_1 & 0 & 0 \end{bmatrix} \quad (3.33)$$

,

$$\mathbf{D} = \begin{bmatrix} 0 & 0 & 0 \\ 0 & 0 & 0 \\ -I_L & I_L & 0 \end{bmatrix} \tag{3.34}$$

In the aforementioned matrices, all parameters except duty cycle of switches D_1 , D_2 , D_4 , and dc value of inductor current I_L are known. For the inductor current, there is following equation:

$$I_L = \frac{I_b}{(D_2 - D_1)} = \frac{-0.9}{0.7186 - 0.59} \tag{3.35}$$

Where I_b is desired value of battery current. So, the unknown parameters of expressed matrices are D_1 , D_2 , and D_4 . The values of switches duty cycle are obtained by steady-state equations

$$\begin{bmatrix} V_{in2} & V_{01} - V_{in2} & V_{02} \\ -V_{01} & V_{01} + R_1 I_b & 0 \\ -V_{02} & V_{02} & R_2 I_b \end{bmatrix} \begin{bmatrix} D_1 \\ D_2 \\ D_4 \end{bmatrix} = \begin{bmatrix} V_{02} + V_{01} - V_{in1} \\ R_1 I_b \\ R_2 I_b \end{bmatrix} \tag{3.36}$$

The transfer function matrix of the converter is obtained from the small signal model as follows:

$$G = C(SI - A)^{-1}B + D \tag{3.37}$$

$$y = Gu \tag{3.38}$$

Where y and u are the system output and input vectors, so the three transfer functions are as follows:

$$\frac{\hat{v}_{01}(s)}{\hat{d}_4(s)} = g_{11} \tag{3.39}$$

$$\frac{\hat{v}_T(s)}{\hat{d}_1(s)} = g_{22} \tag{3.40}$$

$$\frac{\hat{i}_b(s)}{\hat{d}_2(s)} = g_{33} \tag{3.41}$$

Also, it is noteworthy that in battery charging mode when the loads power and battery current have low values, it is possible that the converter goes to discontinuous conduction mode. It is known that dc-dc converters will work in DCM if their inductor dc current be less than their inductor current ripple. So, for the proposed converter in battery charging mode by averaging of the inductor voltage and capacitors current during a switching period, the dc equations can be obtained as follows:

$$V_{in2}D_1 + (V_{01} - V_{02})D_2 + V_{02}D_4 = V_{01} + V_{02} - V_{in1} \tag{3.42}$$

$$-I_L D_2 + I_L = \frac{V_{01}}{R_1} \tag{3.43}$$

$$-I_L D_4 + I_L = \frac{V_{02}}{R_2} \tag{3.44}$$

also, the inductor current ripple in battery charging mode can be expressed as

$$\Delta I_L = \frac{V_{in1}D_1T_s}{L} = \frac{35 * [0.59 * 10^{-4}]}{2.5 * 10{-}3} \tag{3.45}$$

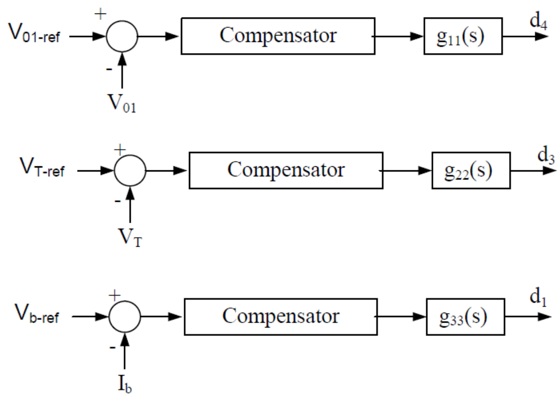

Figure 3.1: Control block diagram of proposed converter battery discharging mode

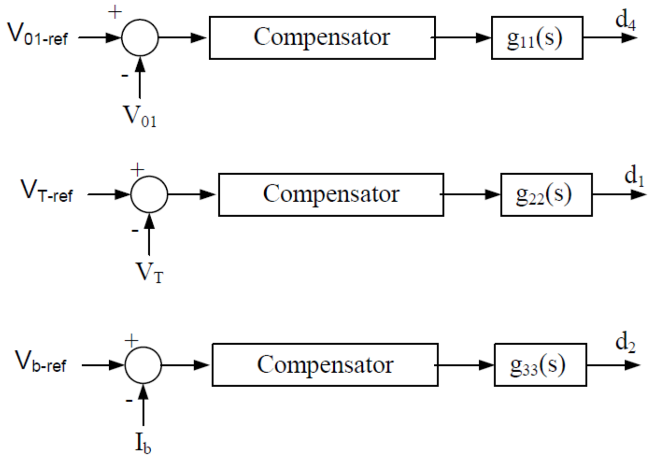

Figure 3.2: Control block diagram of proposed converter battery charging mode

So, from (3.35), (3.42) to (3.44), the converter will work in DCM if the following conditions be satisfied:

$$R_1 > \frac{V_{01} L f_s}{D_1(1 - D_2)V_{in1}} = \frac{80 * 2.5 * 10^{-3} * 10^4}{0.59[1 - 0.7186] * 48} \tag{3.46}$$

$$R_2 > \frac{V_{02} L f_s}{D_1(1 - D_4)V_{in1}} = \frac{48 * 2.5 * 10^{-3}}{0.59[1 - 0.85] * 35} \tag{3.47}$$

$$I_b > \frac{V_{01} D_1 (D_2 - D_1)}{L f_s} = \frac{35 * 0.59 * [0.71 - 0.85]}{2.5 * 10^{-3} * 10^4} \tag{3.48}$$

In fact, (3.46) to (3.48) confirms this fact that the proposed converter will work in DCM when the output loads are light and the battery charging current has low value.

3.4 Summery

Transfer functions of two operation modes of the converter derived in this Chapter . As transfer functions in two operation modes of converter are different, consequently, for each mode, different controller is needed to be designed separately. Controller design will be discuss in chapter 4.

CHAPTER 4

CONTROLLER DESIGN

4.1 Introduction

Transfer functions of two operation modes of the converter derived in Chapter 3. As transfer functions in two operation modes of converter are different, consequently, for each mode, different controller is needed to be designed separately[16],[20]. Hence in this Chapter the controller design is done. In Fig. 3.1 and Fig. 3.2, control block diagrams of converter in two operation mode are shown. In battery discharging mode $R_1 = R_2 = 35\Omega$ and in battery charging mode $R_1 = R_2 = 70\Omega$.

Table 4.1: SIMULATION AND PROTOTYPE PARAMETERS

2.5 mH	L
1000 uF	C_1
1000 uF	C_2
35 V	V_{in1}
48 V	V_{in2}
10 kHz	f_s

4.2 Controller Design for Battery Discharging Mode

As discussed in Chapter 3, in this mode, we have three transfer functions. For each transfer function, frequency-domain bode plot analysis need to be obtained by Matlab to design the system compensators. System compensators should provide desired steady-state error and sufficient phase margin, high stability, and high bandwidth. Utilizing A, B, C, and D matrices which are illustrated in chapter 3 and transfer function matrix G, transfer function of g_{11} is

$$g_{11} = \frac{\hat{v}_{01}(s)}{\hat{d}_4(s)} = \frac{(\frac{V_{02}(1-D_1)}{LC_1})S + (\frac{(1-D_1)V_{02}}{LR_2C_1C_2} - \frac{(1-D_1)(D_4-1)I_L}{LC_1C_2})}{S^3 + (\frac{R_1C_1+R_2C_2}{R_1R_2C_1C_2})S^2 + (\frac{L+(1-D_1)^2R_1C_2R_2+(D_4-1)^2R_1R_2C_2}{LR_1R_2C_1C_2})S + (\frac{R_1(1-D_1)^2+(D_4-1)^2R_2}{LR_1R_2C_1C_2})} \tag{4.1}$$

$$TF = g_{11}(s) = \frac{8.256e^6S + 4.464e^8}{S^3 + 57.14S^2 + 1.986e^6S + 2.622e^6}$$

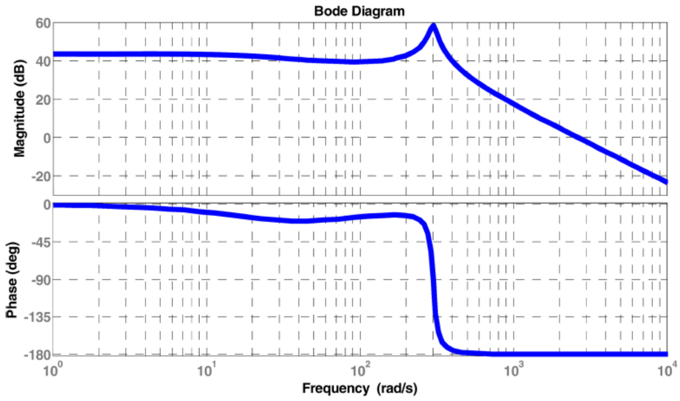

Figure 4.1: Simulated Bode plots of $g_{11}(s)$ before applying the compensator.

Using MATLAB software, the open loop bode diagram of g_{11} for converter simulation parameters which is shown in table I is achieved. Bode diagrams are shown in Fig. 4.1. Investigating the obtained bode plots, it can be understood that in crossover frequency phase of g_{11} is 179.99°. So, the phase margin is not sufficient and closed loop system is unstable. Consequently, to increase phase margin and improve system stability, a lead compensator is designed

$$K(S) = 2.9\frac{S + 906.05}{S + 7641.6} \tag{4.2}$$

In Fig. 4.2, bode diagrams after compensation are shown. It is obvious that by utilizing lead compensator, stability of the system has been provided.

$$TF = g_{11}(s) = \frac{2.394e^7S^2 + 2.299e^{10}S + 1.173e^{12}}{S^4 + 7699S^3 + 2.422e^6S^2 + 1.518e^{10}S + 2e^{10}} \tag{4.2}$$

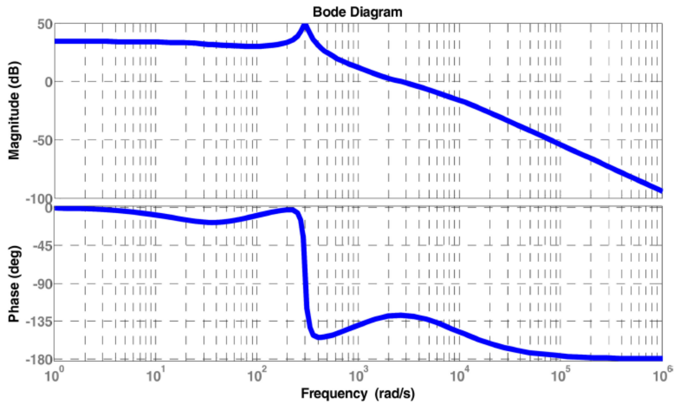

Figure 4.2: Simulated Bode plots of $g_{11}(s)$ after applying the compensator.

Also, transfer function of g_{22} is

$$g_{22} = \frac{\hat{v}_T(s)}{\hat{d}_3(s)} = \frac{(\frac{V_{in2}-V_{in2}}{L})(\frac{(1-D_1)}{C_1} - \frac{(1-D_4)}{C_2})S + (\frac{(1-D_1)}{R_2C_1C_2} - \frac{(D_4-1)}{R_1C_1C_2})(\frac{V_{in2}-V_{in2}}{L})}{S^3 + (\frac{R_1C_1+R_2C_2}{R_1R_2C_1C_2})S^2 + (\frac{L+(1-D_1)^2R_1C_2R_2+(D_4-1)^2R_1R_2C_1}{LR_1R_2C_1C_2})S + (\frac{R_1(1-D_1)^2+(D_4-1)^2R_2}{LR_1R_2C_1C_2})} \tag{4.2}$$

$$TF = g_{22}(s) = \frac{3.333e^6S + 9.523e^7}{S^3 + 57.14S^2 + 1.986e^6S + 2.622e^6}$$

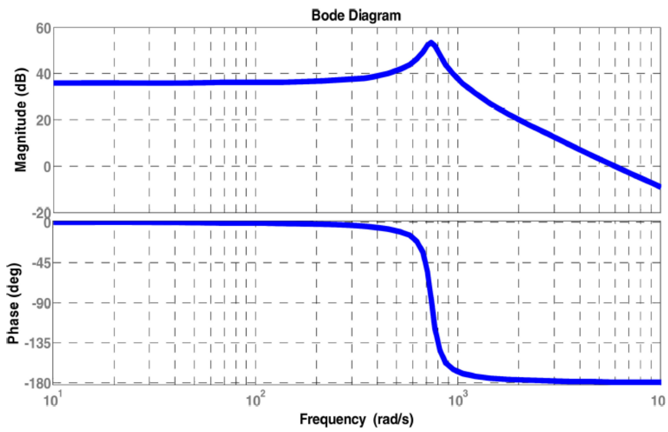

Figure 4.3: Simulated Bode plots of $g_{22}(s)$ before applying the compensator.

In Fig. 4.3, bode diagrams for g_{22} are shown. It can be found from bode diagrams that the phase margin of g_{22} is inadequate, so a lead compensator is required. Consequently, a lead compensator by following transfer function is employed:

$$K_{lead}(S) = 2.8960\frac{S + 2098.9}{S + 16982} \tag{4.2}$$

But using of this lead compensator reduces dc gain and, consequently, leads to increase of steady state error. Conquering this problem, lag compensator is added to system. To avoid the effect of lag compensator on lead compensator, zero of lag compensator is determined ten times smaller than crossover frequency.So, the transfer function of lag is as follows:

$$K_{lag}(S) = \frac{S + 583}{S + 58.345} \tag{4.2}$$

where K = 1, Z= 583.45 and P = 58.345. In Fig. 4.4, bode diagrams after compensation by lead-lag compensators are shown.

$$TF = g_{22}(s) = \frac{9.653e^{6}S^{3} + 2.617e^{10}S^{2} + 1.256e^{13}S + 3.377e^{14}}{S^{5} + 1.71e^{4}S^{4} + 3.95e^{6}S^{3} + 3.39e^{10}S^{2} + 2.012e^{12}S + 2.598e^{12}} \tag{4.2}$$

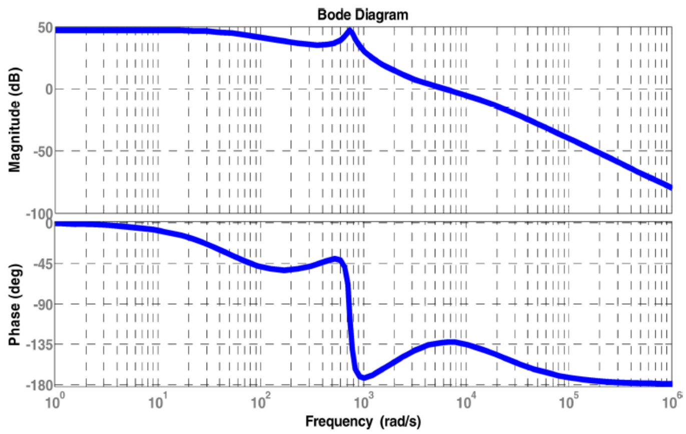

Figure 4.4: Simulated Bode plots of $g_{22}(s)$ after applying the compensator.

As mentioned previously, the current of source 2 (battery) is controlled by switch S_1 . In fact, S_1 controls the inductor current to set the battery current to desired value the related transfer function is shown g_{33} is

$$g_{33} = \frac{\hat{i}_b(s)}{\hat{d}_1(s)} = \frac{(\frac{V_{01}D_3}{L})S^2 + ((\frac{V_{01}D_3}{L})(\frac{1}{R_1C_1} + \frac{1}{R_2C_2}) + \frac{I_L(1-D_1)D_3}{LC_1})S + (\frac{V_{01}D_3}{LR_1R_2C_1C_2} + \frac{I_L(1-D_1)D_3}{LR_2C_1C_2})}{S^3 + (\frac{R_1C_1+R_2C_2}{R_1R_2C_1C_2})S^2 + (\frac{L+(1-D_1)^2R_1C_2R_2+(D_4-1)^2R_1R_2C_1}{LR_1R_2C_1C_2})S + (\frac{R_1(1-D_1)^2+(D_4-1)^2R_2}{LR_1R_2C_1C_2})} \tag{4.2}$$

$$TF = g_{33}(s) = \frac{1.772e^4S^2 + 1.565e^6S + 3.025e^7}{S^3 + 57.14S^2 + 1.986e^6S + 2.622e^6}$$

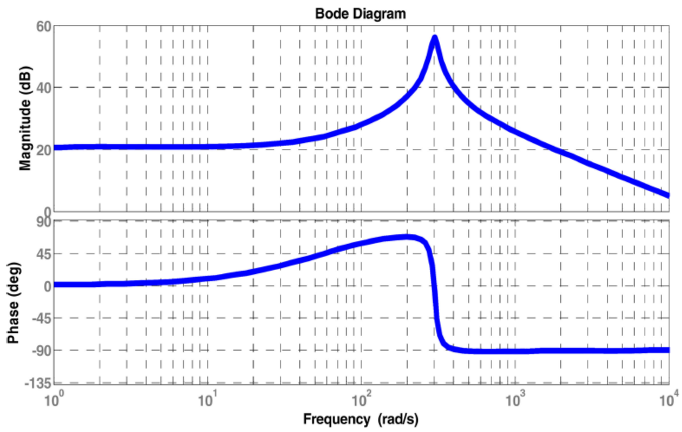

Figure 4.5: Simulated Bode plots of $g_{33}(s)$ before applying the compensator.

Bode diagram of g_{33} is shown in Fig. 4.5 As seen from figure, phase margin is adequate, as result system is stable but the dc gain is low. Consequently, steady-state error has significant value. To reduce steady-state error, a lag compensator is employed

$$K_{lag}(S) = \frac{S + 200}{S + 5} \tag{4.2}$$

$$TF = g_{33}(s) = \frac{1.772e^4S^3 + 5.109e^6S^2 + 3.433e^8S + 6.05e^9}{S^4 + 62.14e^6S^3 + 1.986e^6S^2 + 1.255e^{12}S + 1.311e^7} \tag{4.2}$$

In Fig. 4.6, bode diagrams after applying lag compensator are shown.

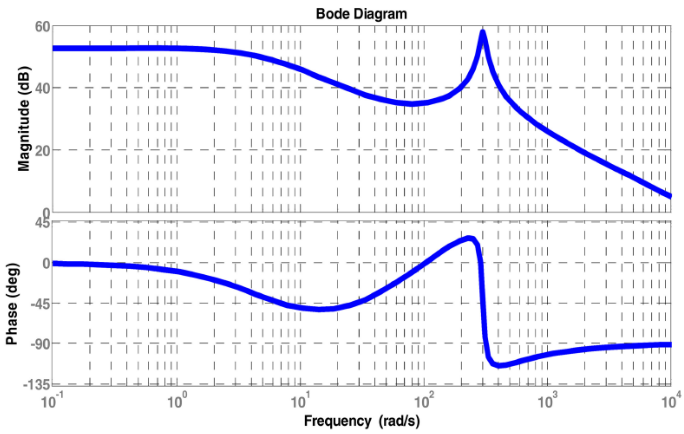

Figure 4.6: Simulated Bode plots of $g_{33}(s)$ after applying the compensator.

4.3 Controller Design For Battery Charging Mode

In this operation mode as cited in previous Chapter, switches S_1 , S_2 , and S_4 are active and S_3 is inactive. In this mode, switch S_4 is used to regulate output voltage V_{O1} , the related transfer function is

$$g_{11} = \frac{\hat{v}_{01}(s)}{\hat{d}_4(s)} = \frac{(\frac{V_{02}(1-D_2)}{LC_1})S + (\frac{(1-D_2)V_{02}}{LR_2C_1C_2} - \frac{(1-D_2)(D_4-1)I_L}{LC_1})}{S^3 + (\frac{R_1C_1+R_2C_2}{R_1R_2C_1C_2})S^2 + (\frac{L+(D_2-1)^2R_1C_2R_2+(D_4-1)^2R_1R_2C_2}{LR_1R_2C_1C_2})S + (\frac{R_1(D_2-1)^2+(D_4-1)^2R_2}{LR_1R_2C_1C_2})} \quad (4.2)$$

$$TF = g_{11}(s) = \frac{7.139e^6S + 1.022e^8}{S^3 + 28.57S^2 + 5.709e^5S + 1.392e^6}$$

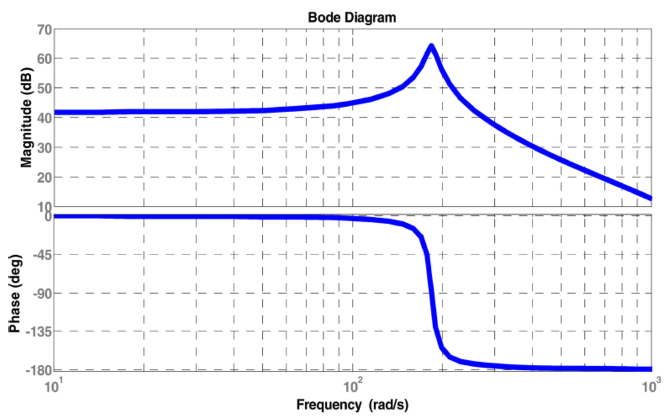

Figure 4.7: Simulated Bode plots of $g_{11}(s)$ before applying the compensator.

Bode diagram of g_{11} is shown in Fig. (4.7). Because of insufficient phase margin, lead compensator is needed. So, lead compensator by following transfer function is designed:

$$K_{lead}(S) = 2.90\frac{S + 482.7}{S + 4065.8} \tag{4.2}$$

To reduce steady-state error following lag compensator is added to system:

$$K_{lag}(S) = \frac{S + 140}{S + 14} \tag{4.2}$$

In Fig. (4.8), bode diagram after applying lead-lag compensator is shown.

$$TF = g_{11}(s) = \frac{2.07e^7S^3 + 1.319e^{10}S^2 + 1.584e^{12}S + 2.003e^{13}}{S^5 + 4108S^4 + 7.444e^5S^3 + 2.332e^9S^2 + 3.818e^{10}S + 7.924e^{10}} \tag{4.2}$$

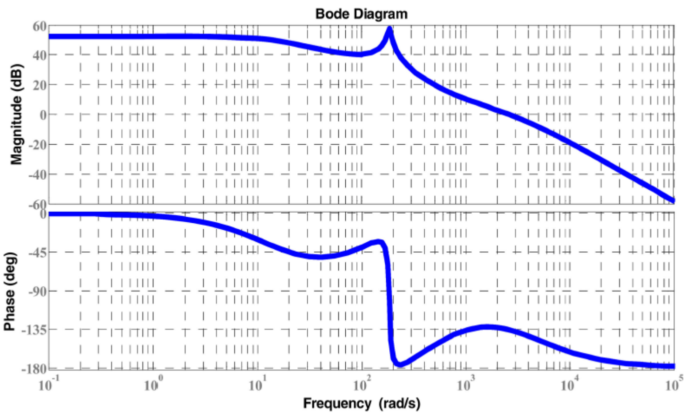

Figure 4.8: Simulated Bode plots of $g_{11}(s)$ after applying the compensator.

Also, in this operation mode, switch S_1 is used to regulate total output voltage V_T , the related transfer function is

$$g_{22} = \frac{\hat{v}_T(s)}{\hat{d}_1(s)} = \frac{(\frac{(1-D_2V_{in2})}{LC_1} + \frac{(1-D_4)V_{in2}}{LC_2})S + (\frac{(1-D_2V_{in2})}{LR_2C_1C_2} + \frac{(D_4-1)V_{in2}}{LR_1C_1C_2})}{S^3 + (\frac{R_1C_1+R_2C_2}{R_1R_2C_1C_2})S^2 + (\frac{L+(D_2-1)^2R_1C_2R_2+(D_4-1)^2R_1R_2C_1}{LR_1R_2C_1C_2})S + (\frac{R_1(D_2-1)^2+(D_4-1)^2R_2}{LR_1R_2C_1C_2})} \tag{4.2}$$

$$TF = g_{22}(s) = \frac{1.152e^7S + 1.314e^8}{S^3 + 28.57S^2 + 5.709e^5S + 1.392e^6}$$

Bode diagram of g_{22} is

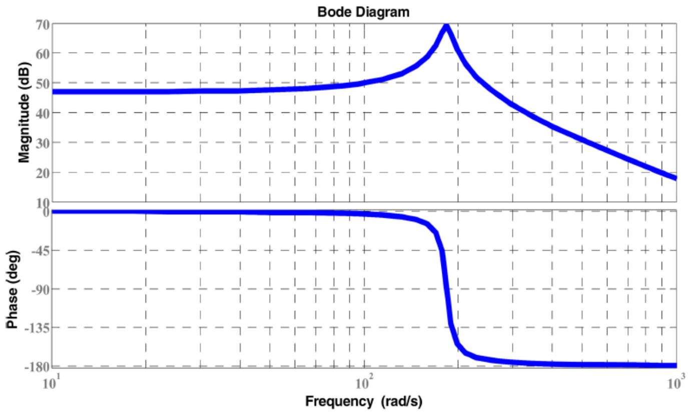

Figure 4.9: Simulated Bode plots of $g_{22}(s)$ before applying the compensator.

Because of insufficient phase margin of g_{22}, following lead compensator is used:

$$K_{lead}(S) = 2.90\frac{S + 585.4}{S + 4937} \tag{4.2}$$

Also, to reduce steady-state error following lag compensator is applied:

$$K_{lag}(S) = \frac{S + 170}{S + 17} \tag{4.2}$$

Bode diagram after compensation is shown.

$$TF = g_{22}(s) = \frac{3.341e^7 S^3 + 2.562e^{10} S^2 + 3.613e^{12} S + 3.793e^{13}}{S^5 + 4983S^4 + 7.964e^5 S^3 + 2.832e^9 S^2 + 5.481e^{10} S + 1.168e^{11}} \tag{4.2}$$

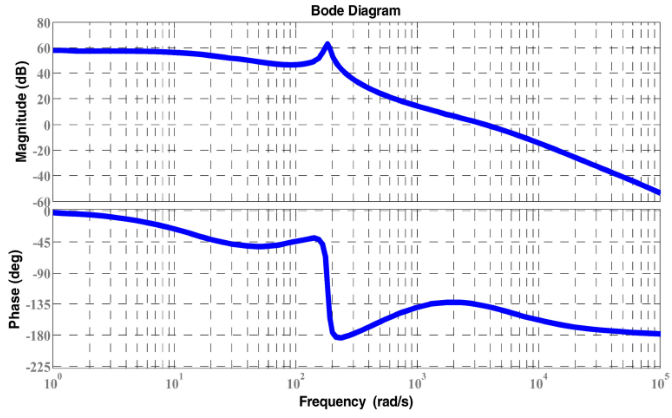

Figure 4.10: Simulated Bode plots of $g_{22}(s)$ after applying the compensator.

Besides, switch S_2 for regulation of battery charging current is used the related transfer function is $g_{33} = \frac{\hat{i}_b(s)}{\hat{d}_2(s)} =$

$$\frac{(\frac{(D_2-D_1)(V_{01}-V_{in2})}{L})S^2+((\frac{(V_{01}-V_{in2})(D_2-D_1)}{L})(\frac{1}{R_1C_1}+\frac{1}{R_2C_2})-\frac{I_L(D_2-D_1)(D_2-1)}{LC_1})S+(\frac{(V_{01}-V_{in2})(D_2-D_1)}{LR_1R_2C_1C_2}-\frac{I_L(D_2-1)(D_2-D_1+I_L}{LR_2C_1C_2}}{S^3+(\frac{R_1C_1+R_2C_2}{R_1R_2C_1C_2})S^2+(\frac{L+(D_2-1)^2R_1C_2R_2+(D_4-1)^2R_1R_2C_1}{LR_1R_2C_1C_2})S+(\frac{R_1(D_2-1)^2+(D_4-1)^2R_2}{LR_1R_2C_1C_2})}$$

$$TF = g_{33}(s) = \frac{1440S^2 + 1.338e^5S + 3.537e^8}{S^3 + 28.57S^2 + 5.709e^5S + 1.392e^6}$$

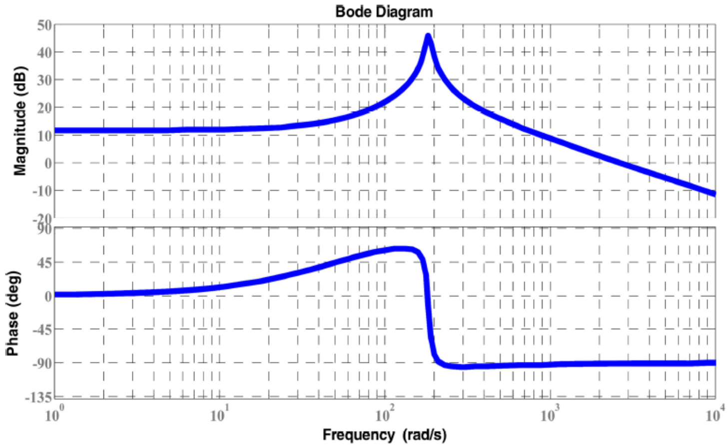

Figure 4.11: Simulated Bode plots of $g_{33}(s)$ before applying the compensator.

Bode diagram of g_{33} is shown in Fig. (4.11). It is obvious from figure that phase margin is sufficient, so there is no need for stabilizing compensator. Just a lag compensator for reducing of steady-state error is used

$$K_{lag}(S) = \frac{S + 267.4}{S + 2.67} \tag{4.2}$$

$$TF = g_{33}(s) = \frac{1440S^3 + 5.19e^5S^2 + 3.714e^7S + 3.537e^8}{S^4 + 31.24S^3 + 5.71e^5S^2 + 2.916e^6S + 3.717e^6} \tag{4.2}$$

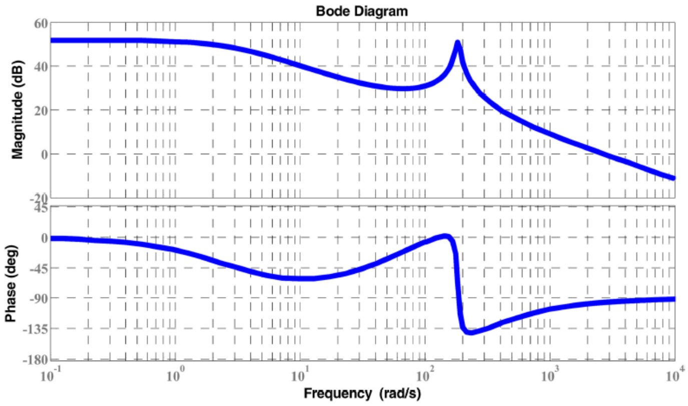

Figure 4.12: Simulated Bode plots of $g_{33}(s)$ after applying the compensator.

4.4 Summery

In this Chapter we have discussed about builting transfer function of system and we analysed about system stability by using Bode plot. We have six transfer functions. For each transfer function, frequency-domain bode plot analysis is obtained by Matlab to design the system compensators. System compensators is provided desired steady-state error and sufficient phase margin,high stability

CHAPTER 5

SIMULATION RESULTS

5.1 Battery Discharging mode

In order to verify the performance of the proposed converter, simulations have been done in battery discharging and charging modes by MATLAB software. The simulation parameters of the converter are listed in Table 5.1.

Table 5.1: SIMULATION AND PROTOTYPE PARAMETERS

2.5 mH	L
1000 uF	C_1
1000 uF	C_2
35 V	V_{in1}
48 V	V_{in2}
10 kHz	f_s

Input voltage sources are considered $V_{in1} = 35$V, $V_{in2} = 48$V. In simulations, battery model is used as input source 2. In this mode switches S_1 , S_3 , and S_4 are active. Each switch is controlled by compensator which is designed in Chapter 4. The output voltages of the converter are desired to be regulated on V_{O1}=80 V and V_{O2}= 40 V. Consequently, total output voltage is desired to be regulated on V_T= 120 V. In Fig. 5.1 voltage V_{O1} is shown.

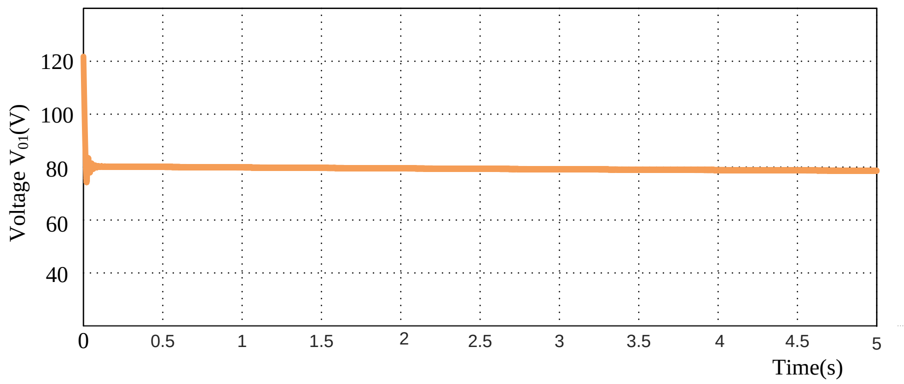

Figure 5.1: Battery discharging mode voltage(V_{O1}) across load R_1

The output voltages is desired to be regulated on V_{02}= 120 V and V_T= 120 V. In Fig.5.2 and Fig.5.3 are shown.

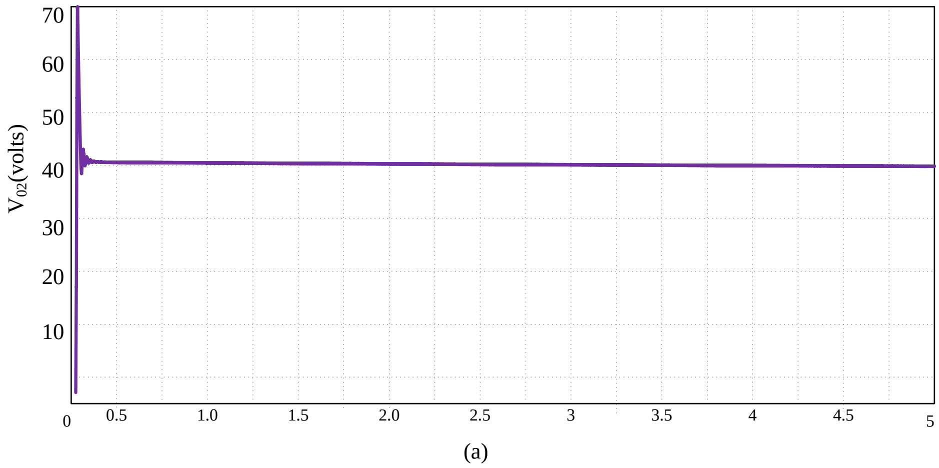

Figure 5.2: Battery discharging mode voltage(V_{O2}) across load R_2

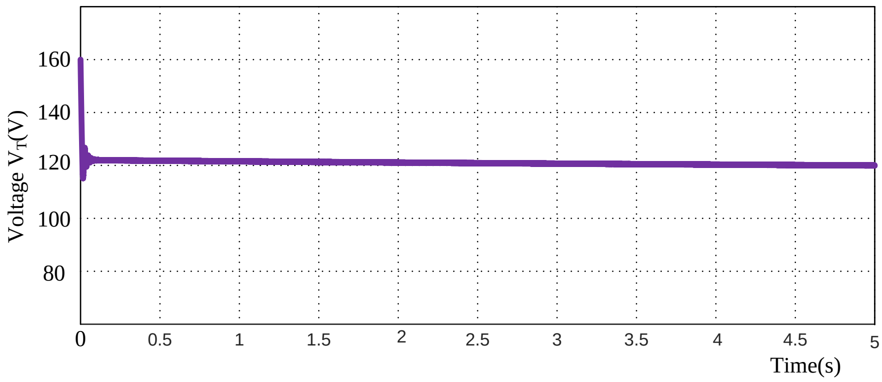

Figure 5.3: Battery discharging mode total output voltage(V_T)

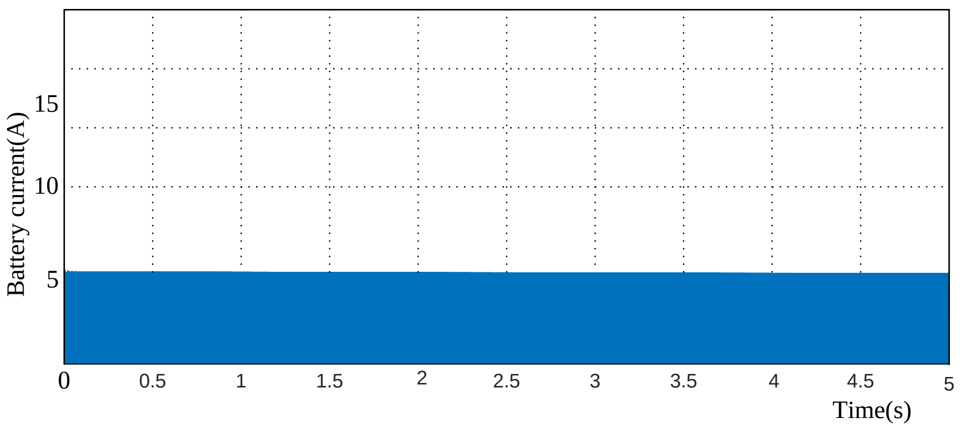

Figure 5.4: Battery current in discharging mode

Battery current is desired to be regulated on I_b= 5.5A and for battery discharging and charging modes, respectively. Load resistances are R_1=R_2= 30Ω for battery discharging mode.

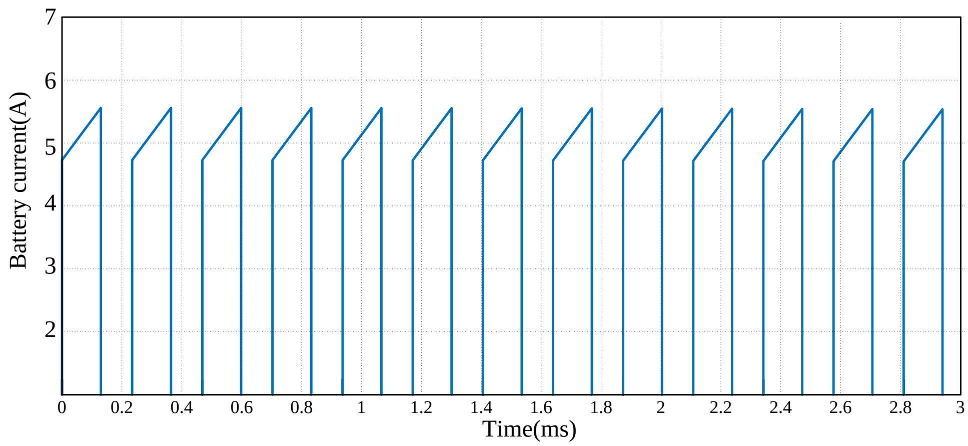

Figure 5.5: Battery current in discharging mode

In Fig. 5.6, inductor current is shown.

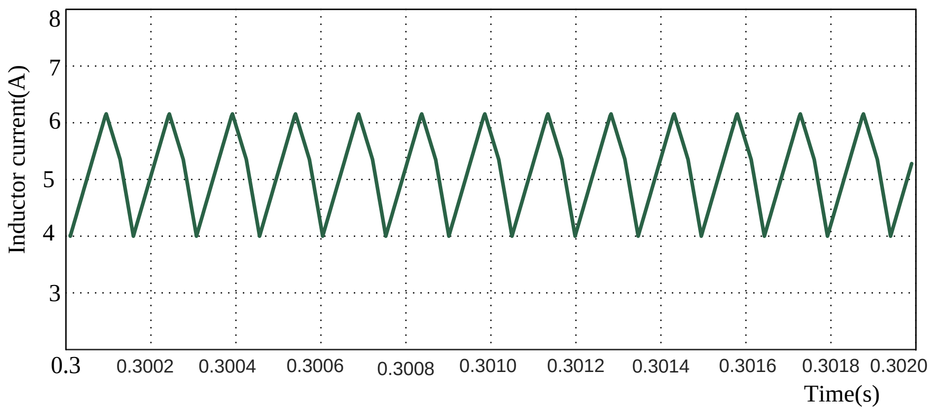

Figure 5.6: Inductor current in battery discharging mode

Output voltages and battery current under these conditions are shown. As seen from this figure, controllers regulated output voltages and battery current. In fact, by controlling battery current, distribution of load power between input sources is feasible.

5.2 Battery charging mode

In battery charging mode, source 1 in addition to supply the loads delivers power to source 2 (battery). In this mode, switches S_1 , S_2 , and S_4 are active. In this mode, similar to battery discharging mode, desired values of output voltages are V_{O1}=80 V, V_{O2}=40 V and V_T=120 V. Load resistances are R_1=R_2= 70Ω. In Fig. 5.7 ,Fig. 5.8 and Fig. 5.9 output voltages are V_{O1} , V_{O2}, V_T are shown.

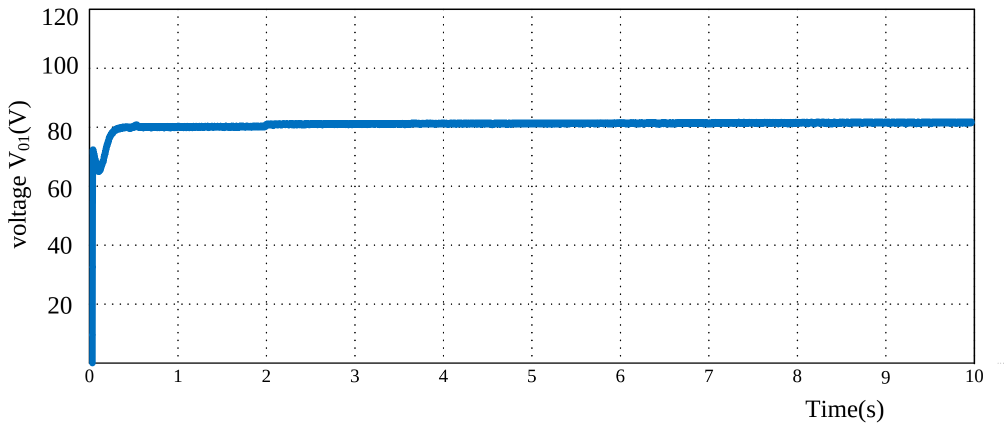

Figure 5.7: Battery charging mode voltage(V_{O1}) across load R_1

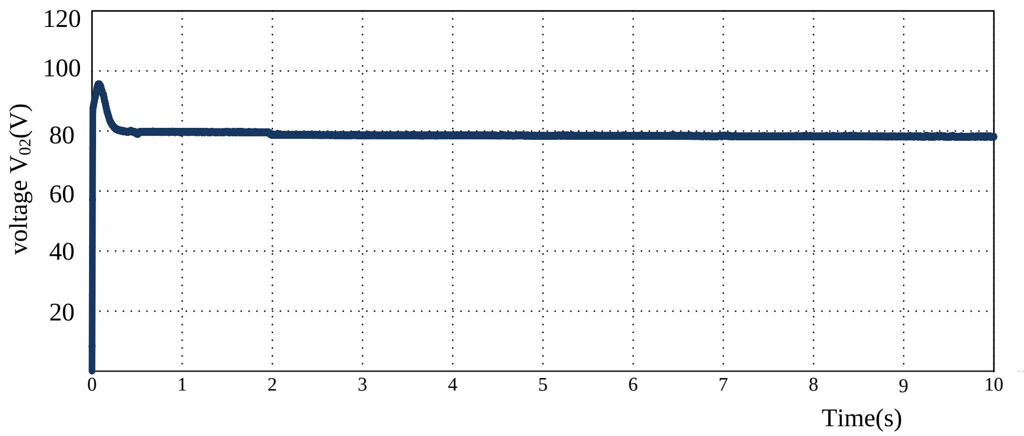

Figure 5.8: Battery charging mode voltage(V_{O2}) across load R_2

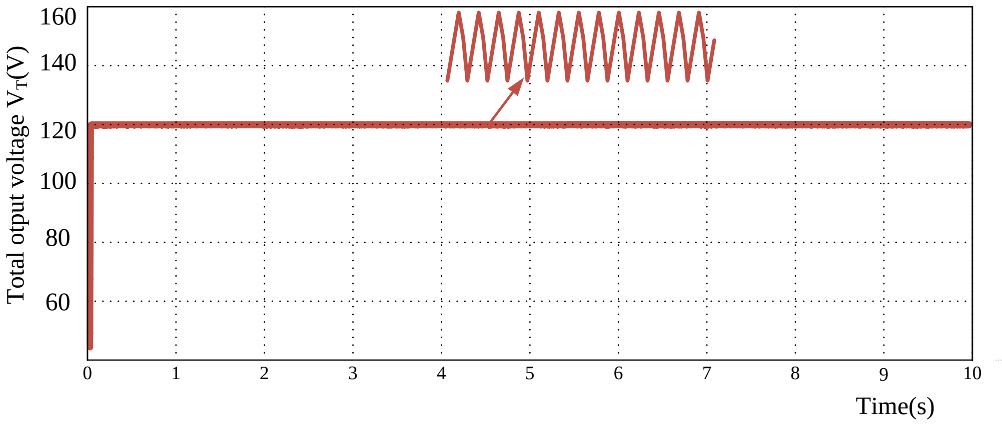

Figure 5.9: Battery charging mode total output voltage(V_T)

Battery charging current reference is $I_b = 0.9$A. In this state, the compensators which are designed for battery charging mode of the converter are used. It is notable that the battery current in this mode has negative value which means the battery has been charged. In Fig. 5.10. battery current is shown.

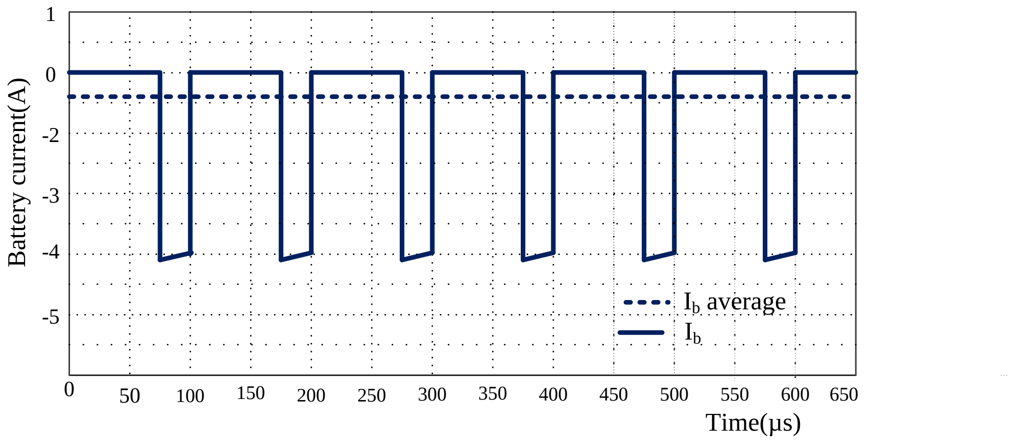

Figure 5.10: Battery Charging mode battery current

In Fig. 5.11. inductor current is shown.

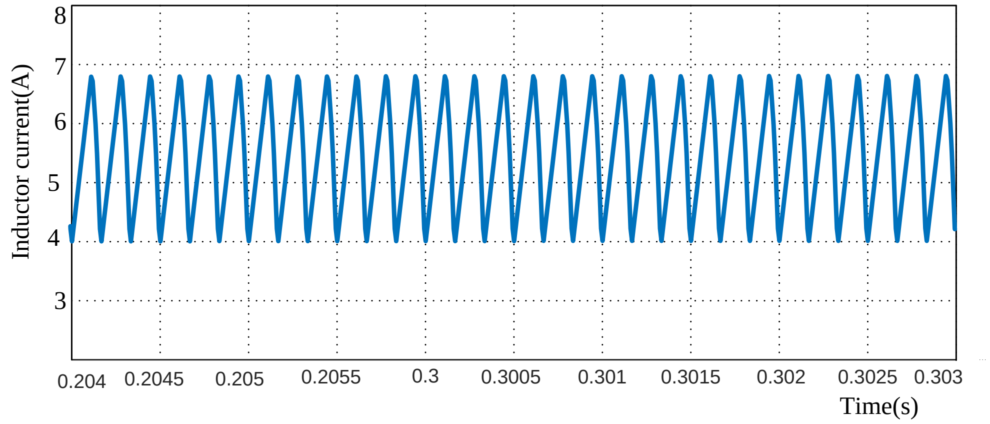

Figure 5.11: Battery charging mode inductor current

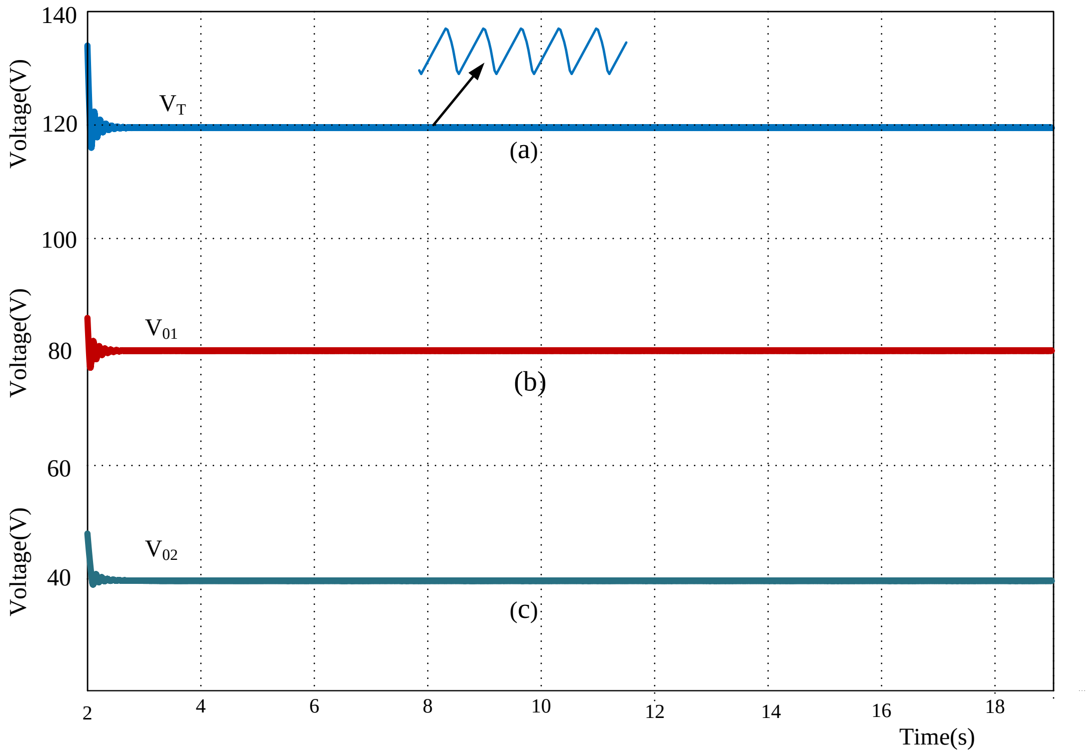

Figure 5.12: After compensation (a) Total voltage V_T (b) Voltage V_{01} (c) Voltage V_{02}

CHAPTER 6

CONCLUSIONS AND SCOPE OF FUTURE WORK

A new multi input multi output DC-DC boost converter with unified structure for hybridizing of power sources in electric vehicles is proposed. The proposed converter has just one inductor. The proposed converter can be used for transferring energy between different energy resources such as FC, PV, and ESSs like battery and SC. FC and battery are considered as power source and ESS, respectively. Also, the converter can be utilized as single input multioutput converter. It is possible to have several outputs with different voltage levels.

The converter has two main operation modes which in battery discharging mode both of input sources deliver power to output and in battery charging mode one of the input sources not only supplies loads but also delivers power to the other source (battery). For each modes, transfer functions matrices are obtained separately and compensators for closed loop control of the converter is designed. It is seen that under various conditions such as rapid rise of the loads power and suddenly change of the battery reference current, output voltages and battery current are regulated to desired values. Outputs with different dc voltage levels are appropriate for connection to multilevel inverters. In electric vehicles, using of multilevel inverters leads to torque ripple reduction of induction motors. Also, electric vehicles which use dc motors have at least two different dc voltage levels, one for ventilation system and cabin lightening and other for supplying electric motor. Moreover, in grid connection of renewable energy resources like PV, using of multilevel inverters is useful.

References

1. X. Zhang and C. Mi, Vehicle Power Management, New York, NY, USA:Springer, 2011.

2. M. Ehsani, Y. Gao, and A. Emadi, Modern Electric, Hybrid Electric and Fuel Cell Vehicle Fundamentals, Theory and Design, 2nd ed., New York, NY, USA: CRC Press, 2010.

3. P. Thounthong, V. Chunkag, P. Sethakul, B. Davat, and M. Hinaje Comparative study of fuel-cell vehicle hybridization with battery or supercapacitor storage device, IEEE Trans. Veh. Technol., vol. 58, no. 8, pp. 38923905, Oct. 2009.

4. L. Wang, E. G. Collins, and H. Li Optimal design and real-time control for energy management in electric vehicles, IEEE Trans. Veh. Technol., vol. 60, no. 4, pp. 14191429, May 2011.

5. M. Zandi, A. Peyman, J. P. Martin, S. Pierfederici, B. Davat, and F.Meybody-tabar Energy management of a fuel cell/supercapacitor/battery power source for electric vehicular applications, IEEE Trans. Veh. Technol.,vol. 60, no. 2, pp. 433443, Feb. 2011.

6. P. Thounthong, S. Pierfederici, and B. Davat, Analysis of differential flatness-based control for fuel cell hybrid power source, IEEE Trans. Energy Convers., vol. 25, no. 3, pp. 909920, Sep.2010.

7. A. Peyman, S. Pierfederici, F. Meybody-tabar, and B. Davat, An adapted control strategy to minimize dc-bus capacitors of parallel fuel cell/ultracapacitor hybrid system, IEEE Trans. Power Electron, vol. 26, no. 12, pp. 38433852, Dec. 2011.

8. M.Michon, J. L. Duarte, M. A. M. Hendrix, and M. G. Simes, At hree port bidirectional converter for hybrid fuel cell systems, in Proc. 35th Annu.IEEE Power Electron. Spec. Conf., Aachen, Germany, 2004, pp.47364741.

9. J. L. Duarte, M. Hendrix, and M. G. Simoes, Three-port bidirectional converter for hybrid fuel cell systems, IEEE Trans. Power Electron., vol. 22, no. 2, pp. 480487, Mar. 2007.

10. H. Tao, A.Kotsopoulos, J. L.Duarte, andM.A.M.Hendrix, Transformercoupled multiport ZVS bidirectional DC-DC converter with wide input range, IEEE Trans. Power Electron., vol. 23, no. 2, pp. 771781, Mar.2008.

11. H. Tao, A. Kotsopulos, J. L. Duarte, and M. A. M. Hendrix, Family of multiport bidirectional DC-DC converters, Inst. Electr. Eng. Proc. Elect. Power Appl., vol. 153, no. 3, pp. 451458, May 2006

12. H. Tao, J. Duarte, and M. Hendrix, Three-port triple-half-bridge bidirectional converter with zero-voltage switching, IEEE Trans. Power Electron.,vol. 23, no. 2, pp. 782792, Mar. 2008.

13. H. Krishnaswami and N. Mohan, Three-port series-resonant DC-DC converter to interface renewable energy sources with bidirectional load and energy storage ports, IEEE Trans. Power Electron., vol. 24, no. 10,pp. 22892297, Oct. 2009.

14. R. Ahmadi and M. Ferdowsi, Double-input converter on h-bridge cells: derivation, small-signal modeling, and power sharing analysis IEEE Trans. Circuit Syst., vol. 59, no. 4, pp. 875889, Apr. 2012.

15. V. A. K. Prabhala, D. Somayajula and M. Ferdowsi, Power sharing in a double-input buck converter using dead-time control, in Proc. Energy Convers. Congr. Expo., 2009.

16. Z. Li, O. Onar, and A. Khaligh, Design and control of a multiple input DC/DC Converter for battery/ultra capacitor based electric vehicle power system in Proc. IEEE Twenty-Fourth Annu. Appl. Power Electron. Conf. Expo., 2009.

17. K. Gummi and M. Ferdowsi, Double-input DC-DC power electronic converters for electric-drive vehicles topology exploration and synthesis using a single-pole triple-throw switch, IEEE Trans. Ind. Electron., vol. 57, no. 2, pp. 617621, Feb. 2010.

18. S. M. Dehghan, M. Mohamadian, A. Yazdian, and F. Ashrafzadeh, Dualinput dual-output Z-source inverter, IEEE Trans. Power Electron., vol. 25, no. 2, pp. 360368, Feb. 2010.

19. T. Bhattacharya, V. S. Giri, K. Mathew, and L. Umanand, Multiphase bidirectional flyback converter topology for hybrid electric vehicles, IEEE Trans. Ind. Electron., vol. 56, no. 1, pp. 7883, Jan. 2009.

20. F. Nejabatkhah, S. Danyali, S. H. Hosseini, M. Sabahi, and S. A. Mozaffari Niapour, Modeling and control of a new three-input DC-DC Boost converter for hybrid PV/FC/battery power system, IEEE Trans. Power Electron., vol. 27, no. 5, pp. 23092325, May 2012.

21. Y. C. Liu and Y. M. Chen, A systematic approach to synthesizing multiinput DC-DC converters, IEEE Trans. Power Electron., vol. 24, no. 1, pp. 116127, Jan. 2009.

22. O. C. Onar and A. Khaligh, A novel integrated magnetic structure based DC/DC converter for hybrid battery/ultracapacitor energy storage systems, IEEE Trans. Smart Grid, vol. 3, no. 1, pp. 296308, Mar. 2012.

23. H. Wu, K. S. Ding, and Y. Xing, Topology derivation of nonisolated three-port DC-DC converters from DIC and DOC, IEEE Trans. Power Electron., vol. 28, no. 7, pp. 32973307, Jul. 2013.

24. S. Danyali, S.H. Hosseini, and G. B. Gharehpetian, New extendable single stage multi-input DC-DC/AC boost converter, IEEE Trans. Power Electron., vol. 29, no. 2, pp. 775788, Feb. 2014.

25. A. Nami, F. Zare, A. Ghosh, and F. Blaabjerg, Multi-output DC-DC converters based on diod-clamped converters configuration: Topology and control strategy, IET Power Electron., vol. 3, pp. 197208, 2010.

26. A. A. Boora, A. Nami, F. Zare, A. Ghosh, and F. Blaabjerg, Voltagesharing converter to supply single-phase asymmetrical four-level diodeclamped inverter with high power factor load, IEEE Trans. Power Electron., vol. 25, no. 10, pp. 25072521, Oct. 2010.

27. J. D. Dasika, B. Bahrani, M. Saeedifard, A. Karimi, and A. Rufer, Multivariable control of single-inductor dual-output buck converters, IEEE Trans. Power Electron., vol. 29, no. 4, pp. 20612070, Apr. 2014.

28. H. Behjati and A. Davoudi, A MIMO topology with series outputs: An interface between diversified energy sources and diode-clampedmultilevel inverter, in Proc. Appl. Power Electron. Conf. Expo., 2012.

29. H. Behjati andA.Davoudi, Amulti-portDC-DC converter with independentcoutputs for vehicular applications, in Proc. Vehicle Power Propulsion Conf., 2011.

30. R.W. Erickson and D. Maksimovic, Fundamentals of Power Electronics.2nd ed., New York, NY, USA: Kluwer Academic Publisher, 2000.